

Nanostructured Metal Oxides and Sulfides for Lithium–Sulfur Batteries

Xue Liu, Jia-Qi Huang, Qiang Zhang,* and Liqiang Mai*

Lithium–sulfur (Li–S) batteries with high energy density and long cycle life are considered to be one of the most promising next-generation energy-storage systems beyond routine lithium-ion batteries. Various approaches have been proposed to break down technical barriers in Li–S battery systems. The use of nanostructured metal oxides and sulfides for high sulfur utilization and long life span of Li–S batteries is reviewed here. The relationships between the intrinsic properties of metal oxide/sulfide hosts and electrochemical performances of Li–S batteries are discussed. Nanostructured metal oxides/sulfides hosts used in solid sulfur cathodes, separators/interlayers, lithium-metal-anode protection, and lithium polysulfides batteries are discussed respectively. Prospects for the future developments of Li–S batteries with nanostructured metal oxides/sulfides are also discussed.

1. Introduction

Lithium–sulfur (Li–S) batteries have been strongly considered in the last six years for their promising future in the practical applications of electric vehicles, unmanned aerial vehicles, satellites, and other energy-storage areas working under harsh conditions.^[1,2] The sulfur cathodes in Li–S batteries afford a very high theoretical specific capacity of 1675 mA h g⁻¹ (more than five times the capacity of the traditional LiCoO₂ cathode) and the Li–S electrochemical pair possesses an energy density of 2600 W h kg⁻¹ or 2800 W h L⁻¹ (up to five times more than conventional lithium-ion batteries at a significantly lower cost).^[3,4]

A comparison of prototypes between Li-ion batteries and Li–S batteries is shown as **Figure 1a**.^[5] A typical Li–S cell undergoes an overall reaction of $16\text{Li} + \text{S}_8 \rightarrow 8\text{Li}_2\text{S}$, where a series of soluble intermediate Li_2S_x ($4 \leq x \leq 8$) are generated.^[2,6,7] The

long chain polysulfides (Li_2S_x ($4 \leq x \leq 8$)) can easily dissolve in the liquid electrolyte, while Li_2S_2 and Li_2S do not. Many efforts have been devoted to research on the reaction mechanism of Li–S batteries from both experiments^[8] and theoretical modeling.^[9,10] A widely accepted illustration of the reaction process of Li–S batteries is shown in **Figure 1b**.^[11] The intermediate reactions are complex with the considerations of complicated reaction pathways of different kinetics combined with parasitic diffusion of polysulfides in a working cell (**Figure 1c**).^[7] Up to now, a simplified reaction sequence of $\text{S}_8 \rightarrow \text{Li}_2\text{S}_8 \rightarrow \text{Li}_2\text{S}_6/\text{Li}_2\text{S}_4 \rightarrow \text{Li}_2\text{S}_2/\text{Li}_2\text{S}$ has been accepted, while some other reaction routes

with the formation of S_3^{2-} and other polysulfide intermediates through disproportionation/decomposition reaction have also been suggested. There are three main obstacles impeding the practical applications of Li–S cells: i) the insulating nature of sulfur and lithium (di)sulfide; ii) the soluble polysulfides generated during the discharge/charge process of a working Li–S cell, which results in the notorious shuttling of the polysulfides; iii) the unstable structure of the Li anode and cathode caused by huge volume fluctuation, which induces dendrite formation and related safety issues.^[12–15]

The first disadvantage influences the 3D continuous conductance of electrons in the cathode. The shuttling effect of polysulfides leads to a low Coulombic efficiency and the rapid degradation of Li–S batteries. The long-chain polysulfides generated in the cathode diffuse to the lithium anode and form short-chain polysulfides or a passive layer on the anode surface, which is the corresponding self-discharge of a cell. The short-chain polysulfides may diffuse back to the cathode and react with elemental sulfur or long-chain polysulfides, which forms a parasitic reaction cycle and lowers the Coulombic efficiency. Meanwhile, the consumption of elemental sulfur in forming the passive layer on the surface of the lithium anode leads to the capacity degradation due to the loss of active materials. The third one destroys the pristine structure of both the sulfur cathode and the lithium anode, which gives rise to the failure of the full cell.

The rational design of composite cathodes with a high sulfur utilization and long life span is the first step to demonstrating the potential of Li–S batteries. With the flourish of controllable fabrication of advanced nanomaterials,^[16,17] the introduction of sulfur to such nanostructures renders composite materials with 3D interlinked electron pathways and interconnected ion-diffusion channels. Conductive nanomaterials exhibit a small

X. Liu, Prof. L. Mai
State Key Laboratory of Advanced Technology
for Materials Synthesis and Processing
International School of
Materials Science and Engineering
Wuhan University of Technology
Wuhan 430070, P. R. China
E-mail: mlq518@whut.edu.cn



X. Liu, Prof. J.-Q. Huang, Prof. Q. Zhang
Beijing Key Laboratory of Green Chemical Reaction
Engineering and Technology
Department of Chemical Engineering
Tsinghua University
Beijing 100084, P. R. China
E-mail: zhang-qiang@mails.tsinghua.edu.cn

DOI: 10.1002/adma.201601759

size, large surface area, tunable porous structure, and unique chemical binding with absorbents, which renders the composites with abundant interfaces where electron and Li ions can meet with the active sulfur for multi-electron conversion reactions. Therefore, the concept of rational design of conductive nanostructured sulfur cathodes is strongly considered.

Herein, we divide the development of composite sulfur cathode into three families. The first family is mainly on the nanostructured carbon as a conductive host material for sulfur, such as microporous carbon,^[18] mesoporous carbon,^[19] micro-meso-macroporous carbon,^[20] carbon fibers,^[21] carbon spheres,^[22] carbon nanotubes,^[23] graphene,^[24] or their hybrids.^[25] Owing to their superb electron pathways and 3D interconnected nature, the carbon materials are very effective to host sulfur and to serve as physical barrier in C/S composite cathodes.^[3,26] This significantly improves the sulfur utilization and affords bulk C/S cathodes for practical Li-S full cells. However, the conjugate nonpolar carbon planes have limited sites to strongly anchor polar molecules (e.g., lithium polysulfides and (di)sulfides).

To provide anchoring sites for chemically binding the polysulfide intermediates, the introduction of polar sites onto carbon planes has been proposed.^[27] Doped carbon with tunable polar sites and effective electron pathways is assigned as the second family. For instance, graphene oxides,^[28] nanostructured carbon (graphene, graphene oxide, carbon nanotubes and so on) materials doped with heteroatoms (N,^[29–32] S,^[32] B,^[33] O,^[30,34] and P^[35]), as well as conductive polymers,^[36] have been extensively explored for Li-S batteries. The carbon chains contribute the conductive scaffolds, and the doped sites or functional groups on the conductive polymers render the chemical anchoring sites.

To further modulate the binding energy with polysulfides and increase the tap density of electrodes, nanostructured polar inorganic compounds, such as transitional-metal oxides, sulfides, and carbides have emerged as polar host materials toward lithium (poly)sulfides. This is the third family: scaffolds that are constituted by nanostructured inorganic compounds. These compounds (such as Ti₂C,^[32] TiC,^[37] Ti₄O₇,^[38,39] and CoS₂,^[40]) have much stronger adsorption ability to polysulfides and render the Li-S cells with high sulfur utilization and long life span. Nanostructured oxides and sulfides with a controllable exposed surface and 3D nanoarchitectures are expected to afford efficient and effective anchoring sites for polysulfides in working Li-S batteries. However, compared to energy materials employed in the first two families, those in the third strategy are less investigated at the moment. Moreover, the areal sulfur loading and rate capability of Li-S batteries should be enhanced when nanostructured inorganic compounds are applied in a working cathode.

Here, recent advances in the use of nanostructured oxides and sulfides for Li-S batteries are reviewed. Nanostructured oxides and sulfides are demonstrated to be effective conductive polar host materials that adsorb polysulfides efficiently during the discharge and avoid the detachment of lithium (di)sulfides into the electrolyte. Moreover, these inorganic host materials can also render the possibility of accelerating the conversion process of lithium polysulfides to lithium (di)sulfides or the inverse process. We describe metal oxides as additives for solid sulfur cathodes, focusing on their interactions with polysulfides and briefly on the synthesis. We further follow up to discuss sulfiphilic sulfide materials. Except for solid sulfur cathodes, the



Xue Liu obtained his Bachelor's degree in 2014 from the School of Materials Science and Engineering, Wuhan University of Technology. He is now a Ph.D. candidate at Wuhan University of Technology with Prof. Liqiang Mai and also a visiting student in Prof. Qiang Zhang's group in the Department of Chemical Engineering, Tsinghua University. His research interests focus on cathode materials for Li-S batteries and nano-carbon materials.



Qiang Zhang received his bachelors and Ph.D. degrees from Tsinghua University in 2004 and 2009, respectively. After a stay as a research associate at Case Western Reserve University, USA, he joined the Fritz Haber Institute of the Max Planck Society, Germany. He was appointed an associate professor at Tsinghua University at 2011. His interests focus on energy materials, including 3D nanocarbon, Li-S batteries, and oxygen electrocatalysis.



Liqiang Mai received his Ph.D. degree from Wuhan University of Technology in 2004. He then carried out postdoctoral research in the laboratory of Prof. Zhonglin Wang at Georgia Institute of Technology in 2006–2007 and worked as an advanced research scholar in the laboratory of Professor Charles M. Lieber at Harvard University in 2008–2011. He is Chair Professor of Materials Science and Engineering at Wuhan University of Technology. His interests include nanowire materials, micro-/nano-energy-storage devices, and energy-based nano-bio interfaces.

use of metal oxides and sulfides in related Li-S systems is also included.

2. Nanostructured Oxides for Li-S Batteries

Metal oxides that typically contain an anion of oxygen in the oxidation state of O²⁻ are always with a strong polar surface.

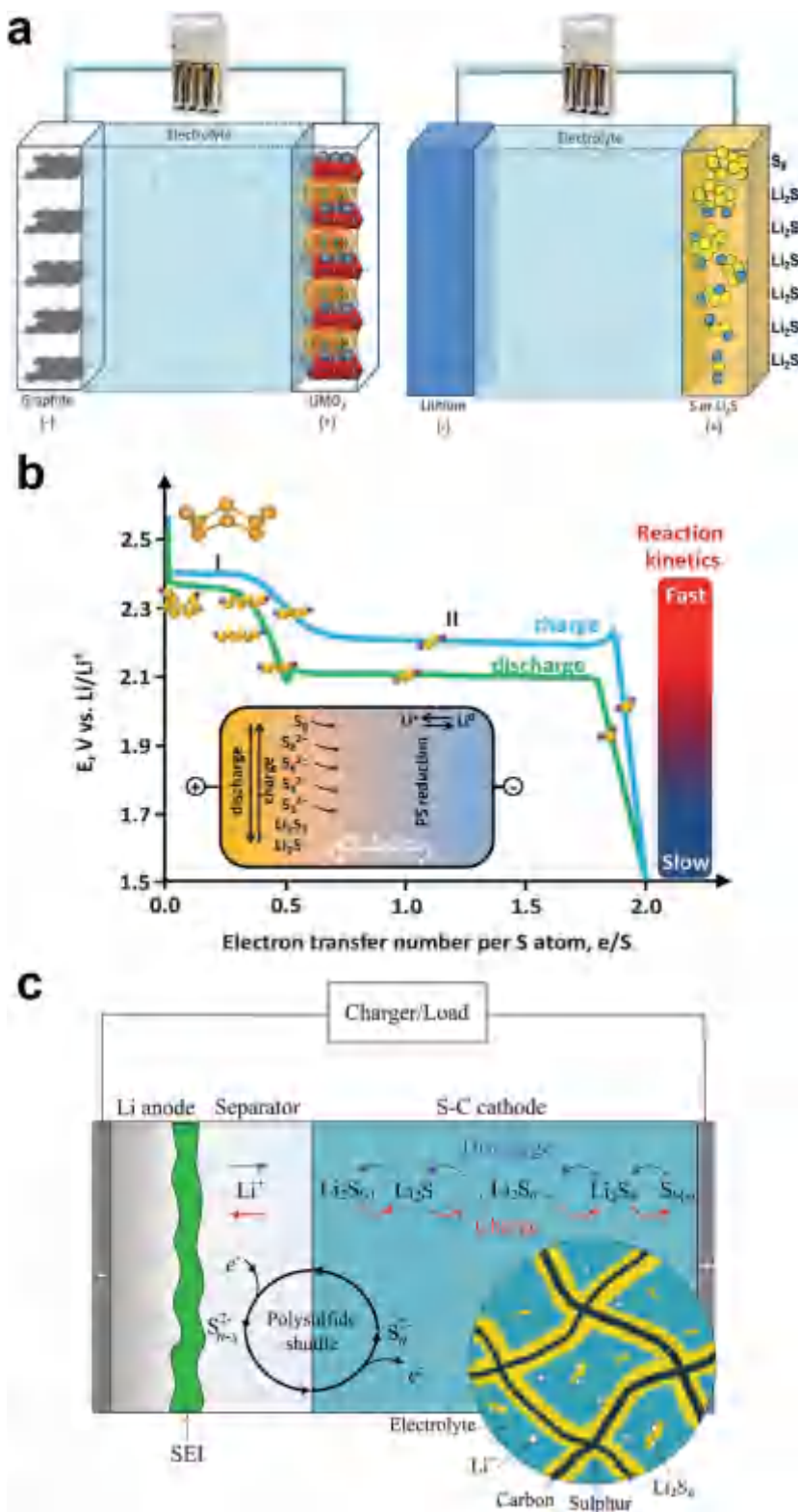


Figure 1. a) Schematic representation of Li-ion batteries based on the intercalation reaction (left) and Li-S batteries based on the conversion reaction (right). b) An ideal charge-discharge curve with different sulfur-containing species at different stages, the inset presents the polysulfide shuttling mechanism. c) Illustration of the dissolution and shuttling of polysulfides in a Li-S cell. a) Reproduced with permission.^[5] Copyright 2015, Wiley-VCH.

Because of the strong binding between the oxygen and the metal, metal oxides tend to be insoluble in most organic solvents. Early studies on the nonconductive polar oxides used in Li-S batteries are all based on the modifications of nanostructured carbon/sulfur cathodes with oxides. For instance, the nanosized Mg_{0.6}Ni_{0.4}O additive was the first reported oxide used in cathodes in absorption of polysulfides for Li-S batteries.^[41] SiO₂ has been used as an effective polysulfide reservoir material^[42] in CMK-3/sulfur cathodes to improve the discharge capacity and cycling performances of Li-S cells. Therefore, nonconductive oxide nanostructures are directly added to the cathode with the role of an additive (less than 10 wt%). Compared to nanostructured carbon materials, metal oxides afford abundant polar active sites for absorption of polysulfides. Attributed to the intrinsic defects and unique band structures, some metal oxides even have good conductivity. Moreover, the volumetric energy density of Li-S cells is significantly improved through the engineering fabrication of nanostructured metal oxides and sulfur composites because of the high intrinsic density of oxides in comparison with nanocarbon materials. Therefore, a few metal oxides are proposed as conductive hosts for Li-S batteries. In this section, we will review some typical metal oxides (e.g., TiO₂, Ti₄O₇, MnO₂, and NiFe₂O₄) to demonstrate the potential of oxides for Li-S batteries.

2.1. TiO₂

TiO₂ is a naturally occurring oxide of titanium. Generally, it is sourced from anatase (α -TiO₂), rutile (β -TiO₂), brookite (γ -TiO₂), and Bronze B (Figure 2a).^[43] Titanium dioxide nanomaterials with zero-dimensional (0D), 1D, 2D, and 3D nanostructures have been widely used in paint, sunscreen, photocatalysts, photovoltaics, sensors, lithium-ion batteries, biomedical applications, and so on. Due to its polar surface, TiO₂ has also been applied as a host material in Li-S batteries.

Oxide additives to the cathode in Li-S batteries were primarily investigated by Nazar and co-workers.^[45] Nanocrystalline mesoporous α , β , and γ -TiO₂ were proposed

b) Reproduced with permission.^[11] Copyright 2013, Royal Society of Chemistry. c) Reproduced with permission.^[7] Copyright 2015, Royal Society of Chemistry.

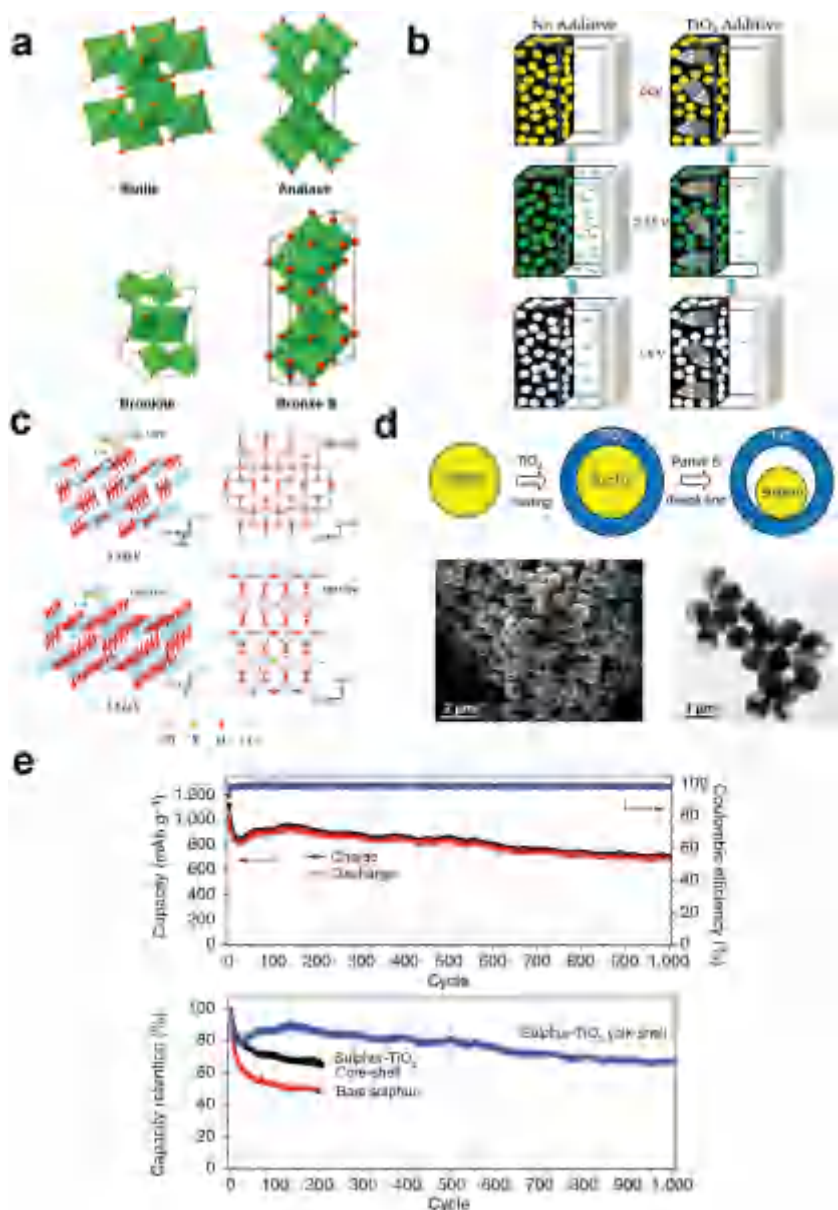


Figure 2. The use of TiO₂ in the cathode for Li-S batteries. a) Four common polymorphs of TiO₂. b) A schematic diagram illustrating the concept of a Li-S cell with polysulfide reservoirs vs no reservoirs at different stages of discharge. c) An adsorption configuration of Li₂S on the surfaces of anatase-TiO₂ (101) and rutile-TiO₂ (110), obtained from DFT calculations. d) A typical synthesis process and SEM, TEM characterizations of sulfur-TiO₂ yolk-shell nanostructures. e) Electrochemical performance of sulfur-TiO₂ yolk-shell nanostructures and control samples. a) Reproduced with permission. Copyright 2016, Royal Society of Chemistry.^[44] b) Reproduced with permission.^[45] Copyright 2015, American Chemical Society. c) Reproduced with permission.^[46] Copyright 2016, Royal Society of Chemistry. d,e) Reproduced with permission.^[47] Copyright 2012, Nature Publishing Group.

as polysulfide reservoirs (Figure 2b) and the role of surface adsorption vs pore absorption has been demonstrated. α , β , and γ -TiO₂ were controlled with a similar surface area but different pore sizes. The sulfur cathode fabricated with the co-heating of mesoporous carbon and sulfur at 155 °C with α -TiO₂ as the additive exhibited the highest 82% C₁₀₀/C₁₀ (where C₁₀₀ and C₁₀ mean the capacity at the 100th and the 10th cycles, respectively)

ratio and a superior initial specific capacity of 1201 mA h g⁻¹ at 1.0C. Batteries with β -TiO₂ as a cathode additive delivered a lower initial and overall specific capacity. In contrast, cells with γ -TiO₂ as the cathode additive exhibited much worse cycling stability and lower initial specific capacity. This is attributed to the poor polysulfide absorption properties on β -TiO₂ particles, which reduces the anchoring effect in retaining polysulfides. The worst battery performance with γ -TiO₂ as the cathode additive hints at the strong anchoring of polysulfides through chemical absorption.

Recent theoretical predictions^[46] on the interactions between TiO₂ and Li₂S indicate that the binding strength of Li₂S to the α -TiO₂ (101) surface (3.59 eV) is a little smaller than β -TiO₂ (110) (3.62 eV) (Figure 2c). The binding energy of the sulfur-containing species to the α -TiO₂ (101) surface (2.30 eV) is higher than that on the β -TiO₂ (110) surface (2.18 eV), and is much higher than that on the surface of graphene (<1.0 eV). This is in accordance with the similar electrochemical performance of α -TiO₂ and β -TiO₂ applied in Li-S cells. Further theoretical predictions on different polymorphs of TiO₂ for Li-S battery applications are strongly considered.

Nanostructured TiO₂ with different morphologies have then been investigated as cathode host materials in Li-S batteries, such as mesoporous hollow TiO₂ spheres,^[48] TiO₂ nanofibers,^[49] nanoparticles,^[50] nanotubes,^[51] and so on. A sulfur-amorphous-TiO₂ yolk-shell structure for the sulfur cathode of Li-S batteries was reported by Cui and co-workers.^[47] The core-shell nanostructures (Figure 2d) were fabricated through the hydrolysis of titanium diisopropoxide bis(acetylacetonate) in a colloidal sulfur suspension with a low amount of poly(vinylpyrrolidone) as surfactant. Toluene was employed to dissolve part of the sulfur in the core-shell particles to create yolk-shell sulfur-TiO₂ nanoparticles. An initial specific capacity of 1030 mA h g⁻¹ at 0.5C and a Coulombic efficiency of 98.4% over 1000 cycles with a capacity decay rate as small as 0.033% per cycle after 1000 cycles were achieved (Figure 2e). The superb electrochemical performance is attributed to there being sufficient free space to allow for volume expansion of the sulfur and the effective function of TiO₂ with a small pore size in minimizing the polysulfide dissolution. Both hydrophilic Ti-O groups and surface hydroxyl groups in TiO₂ are believed to bind favorably with polysulfide anions.

Hydrogen-reduced TiO₂ inverse opals have also been employed as a host for sulfur.^[52] With TiO_{2-x}-encapsulated sulfur, the composite cathode delivered an initial specific

capacity of 1201 mA h g⁻¹ at 1.0C. Batteries with β -TiO₂ as a cathode additive delivered a lower initial and overall specific capacity. In contrast, cells with γ -TiO₂ as the cathode additive exhibited much worse cycling stability and lower initial specific capacity. This is attributed to the poor polysulfide absorption properties on β -TiO₂ particles, which reduces the anchoring effect in retaining polysulfides. The worst battery performance with γ -TiO₂ as the cathode additive hints at the strong anchoring of polysulfides through chemical absorption.

capacity of 1100 mA h g⁻¹ and a reversible specific capacity of 890 mA h g⁻¹ after 200 cycles at a charge/discharge rate of 0.2C. X-ray photoelectron spectroscopy (XPS) results confirm the existence of Ti³⁺ ions and oxygen vacancies, which result in improved electrical conductivity (Figure 3a). There is no Ti⁴⁺/Ti³⁺ transformation during the lithiation/delithiation process. The use of reduced TiO₂ brings several advantages: i) a dramatic increase in electrical conductivity is achieved after hydrogen reduction; ii) both the 3D framework and the thin TiO₂ shell facilitate rapid electron and lithium-ion transport; iii) the generated oxygen vacancies promote the interaction between the TiO₂ and the sulfur, which renders the rational integration of physical confinement and chemical absorption of polysulfides in a working cell. An in situ visual-electrochemical study on a sulfur/hydrogen-reduced TiO₂ (H-TiO₂) electrode (Figure 3b) demonstrated that H-TiO₂ is effective in restricting and capturing polysulfides.^[53]

Along this line, hydrogen-reduced hierarchical mesoporous spheres constructed from anatase nanosheets have been employed in sulfur cathodes.^[46] With its highly exposed (001)

facets, a largest absorption energy of -2.93 eV between S₄²⁻ and TiO₂ is revealed by the density functional theory (DFT) calculations (Figure 3c). S₄²⁻ is likely to be trapped at oxygen defective sites and coordinate with two Ti³⁺ sites. This is the main reason that TiO₂ can anchor polysulfides with the oxygen defects and Ti³⁺ performs well as a cathode host material or a host in barrier layers.

It should be noticed that conductive agents (e.g., carbon black, and CNTs) have been always introduced for slurry preparation. If the TiO₂ is attached to nanocarbon directly, a TiO₂/carbon hybrid is achieved with conductive nonpolar substrates with exposed polar oxygen on the surface of TiO₂. For instance, coupled with carbon nanotubes, hollow TiO₂ was webbed with carbon nanotubes (HMT@CNT) and employed as a sulfur supporter in the cathode of a Li-S cell.^[54] The composite material after etching of TiO₂ was mixed with multi-walled CNTs and then used as an interlayer (named DF-PCW). The high electronic conductivity (four-probe conductivity is 0.14 S cm⁻¹) ensures high rate performances of Li-S cells employing an HMT@CNT/sulfur composite as the cathode and DF-PCW

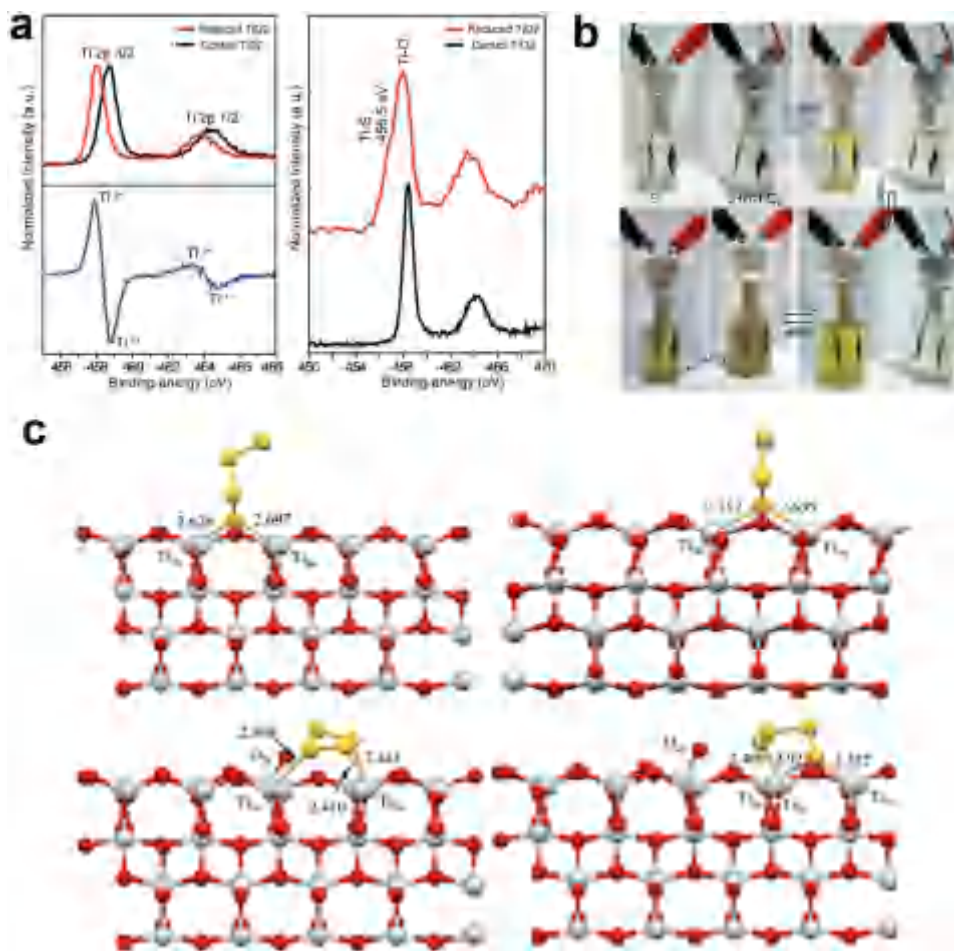


Figure 3. The polysulfide anchoring mechanism on TiO₂. a) The normalized Ti 2p XPS spectra of reduced TiO₂ (red solid curve), control TiO₂ (black solid curve), and their subtraction spectrum (green solid curve) (left) and polysulfides-treated TiO₂ (right). b) A visual confirmation of restricting and recapturing polysulfides. c) Four optimized adsorption models illustrating the interaction between S₄²⁻ and hydrogen-reduced TiO₂ (001) planes with an O_{2c} oxygen vacancy. a) Reproduced with permission.^[52] Copyright 2014, American Chemical Society. b) Reproduced with permission.^[53] Copyright 2014, Nature Publishing Group. c) Reproduced with permission.^[46] Copyright 2016, IOP Publishing.

as the interlayer. 931 mA h g⁻¹ and 888 mA h g⁻¹ at 5.0C and 7.0C rates were achieved, respectively. The polarization of the cell was 383 mV and 485 mV at those rates, respectively. Other TiO₂-modified nanostructured carbon/sulfur materials were also investigated afterward: carbon aerogels,^[55] active carbon,^[56] 3D hierarchical ordered mesoporous carbon,^[57] hollow carbon fibers,^[12] and carbon paper.^[58]

As one of most controllable and safe nanomaterials, TiO₂ is the most investigated oxide host for Li-S batteries. Compared with carbon and conducting macromolecules, S₄²⁻ is likely to be trapped at oxygen defect sites and coordinate with two Ti³⁺ sites. The surface defects and terminated atoms play a decisive role in strong anchoring of polysulfides. However, attributed from the intrinsic poor conductivity of TiO₂, conductive agents have to be introduced rationally to afford efficient use of chemical interactions between TiO₂ and polysulfides for Li-S cells with high sulfur utilization and long life span.

2.2. Ti₄O₇

Based on the effective entrapment of polysulfides in sulfur cathodes through defective TiO₂, the sulfiphilic and metallic oxide host Ti₄O₇ was proposed and proven to be effectively multifunctional when used in cathode of Li-S batteries.^[38] Nazar and co-workers introduced a high-surface-area Magnéli phase oxide Ti₄O₇ with a theoretical bulk conductivity of 2 × 10³ S cm⁻¹ at 298 K (about three fold greater than graphite) as a metallic and polar host for Li-S batteries. The Ti₄O₇ has a surface area of 290 m² g⁻¹ and an electrical conductivity of 3.2 ± 0.1 S cm⁻¹. Thanks to its superior intrinsic capability to absorb polysulfides, the Li₂S₄ (in tetrahydrofuran) solvent with addition of Ti₄O₇ became light yellow immediately, while other samples remained intense yellow-gold (Figure 4a). There is a +2.7 and +1.7 eV shift for S_T⁻¹ and S_B⁻¹, respectively, in the binding energy of XPS spectra (Figure 4b), indicating that strong interaction of both the terminal and bridging sulfur in the LiPSs with the Ti₄O₇ surface results in the polarization of electrons away from the sulfur atoms to the electropositive titanium and/or oxygen vacancies at the interface. Comparative operando X-ray absorption near-edge structure studies on the Ti₄O₇/S electrode and VULCAN XC72 carbon/S (VC/S) electrode corroborate that Ti₄O₇ plays a vital role in the process of surface-mediated reduction of the sulfide species (Figure 4c). As shown in Figure 4d, the Ti₄O₇/S composites with 60 wt% sulfur (Ti₄O₇/S-60) exhibited an initial specific capacity of 1069 mA h g⁻¹ at 0.2C, an 88% capacity retention over 100 cycles at 0.5C, and a decay rate of 0.08% per cycle. Long-term cycling testing of the Ti₄O₇/S-60 cathode delivered an initial specific capacity of 850 mA h g⁻¹ with only 0.06% decay per cycle at 2.0C. An average Coulombic efficiency of ca. 96% for the Ti₄O₇/S-60 composite (versus 80% for a VC/S-60 cathode) was observed in cells without LiNO₃ additive.

Cui and co-workers reported a series of Ti_nO_{2n-1} nanomaterials with strong sulfur binding and conducting Magnéli phase for improving Li-S batteries.^[39] After hydrogen reduction of the as-prepared TiO₂ nanotubes, the Magnéli phase Ti₆O₁₁, of high purity, in a deep purple powder, was obtained. Deep black Ti₄O₇ powder was fabricated at a higher temperature. The

reduction degree enables fine-tuning of the electrical conductivity, showing either semiconductor (Ti₆O₁₁) or metallic (Ti₄O₇) behavior at room temperature. The surface Ti atoms and O vacancies on defective TiO_{2-x} are absorbing sites for the oxide or oxygen species.^[59] There are many differences in the most stable surface structures of Magnéli phase Ti₄O₇ and rutile TiO₂. As shown in Figure 5a, the coordination numbers of Ti on the surface of (1-20) plane of Ti₄O₇ are 4(Ti_{4c}), 5(Ti_{5c}), and 6(Ti_{6c}) and the ratio of Ti_{6c} is only 37.5%. Namely, there are 62.5% surface Ti atoms with unsaturated chemical bonding, whereas on the surface layer of TiO₂ (110), the ratio of Ti_{5c} and Ti_{6c} is 1:1. For Magnéli phase Ti₄O₇, the ensemble of low-coordinated Ti (such as Ti_{5c}) arranges in step sites on Ti₄O₇ (1-20). They are easily accessible, to form external chemical interactions. Meanwhile, for rutile TiO₂, the through line Ti_{5c} on TiO₂ (110) exists at the terrace sites. The most stable surface structure endows Ti₄O₇ (1-20) with the strong binding between sulfur and polysulfide species. Ti₄O₇ is the most suitable among the three chosen materials for cathode anchoring materials. Ti₄O₇-S and Ti₆O₁₁-S exhibited higher discharge capacities of 1108 and 1342 mA h g⁻¹ and a high initial Coulombic efficiency of 91 and 96% at 0.02C in the electrolyte without LiNO₃, respectively. An obvious overcharge was detected on the TiO₂-S electrode. The TiO₂-S cathode exhibited a discharge capacity of 824 mA h g⁻¹ and a Coulombic efficiency of 78%. Moreover, the Ti₄O₇-S composite afforded a very high volumetric capacity of 1580 mA h cm⁻³. Prolonged cycling of Ti₄O₇-S sample at 0.5C displayed an initial discharge capacity of 623 mA h g⁻¹ and retained capacity as high as 604 mA h g⁻¹ after 250 cycles with the capacity decay of only 0.012% per cycle. As shown in Figure 5b, Nyquist plots for the three samples with different titanium oxides confirmed that Ti₄O₇-S sample exhibits the minimum charge-transfer resistance compared with Ti₆O₁₁-S and TiO₂-S, which is attributed to the higher conductivity of Ti₄O₇. Figure 5c shows DFT calculation results of bonding properties of S_x (x = 1, 2, and 4) and Li₂S_x (x = 1, 2, and 4) on Ti₄O₇ (1-20) and TiO₂ (110). The low-coordinated Ti on titanium oxide can stabilize sulfur clusters, whereas oxygen-rich titanium oxide can stabilize metal clusters due to the formation of strong chemical bonding.

The metallic Magnéli phase Ti₄O₇ affords a sulfiphilic surface, which is a promising polar host for the complex multi-electron Li-S conversion reaction. The low-coordinated Ti stabilizes the sulfur clusters, whereas the oxygen-rich area anchors lithium polysulfides and (di)sulfides due to the formation of strong chemical bonding. However, the fabrication of Ti₄O₇ is still very complex: a high-temperature reduction at over 1000 °C is always required. How to guarantee the nanostructures of precursors and achieve Magnéli phase Ti₄O₇ is little studied as yet. The assembly of Magnéli Ti₄O₇ into 3D interconnected conductive and flexible frameworks is still a huge challenge.

2.3. MnO₂

The brown MnO₂ is the main ore of manganese. It has been widely applied in alkaline batteries and the zinc-carbon batteries. There are α, β, γ, and δ-MnO₂ phases (Figure 6a).^[60] The α-polymorph of MnO₂ has an open structure with "channels"

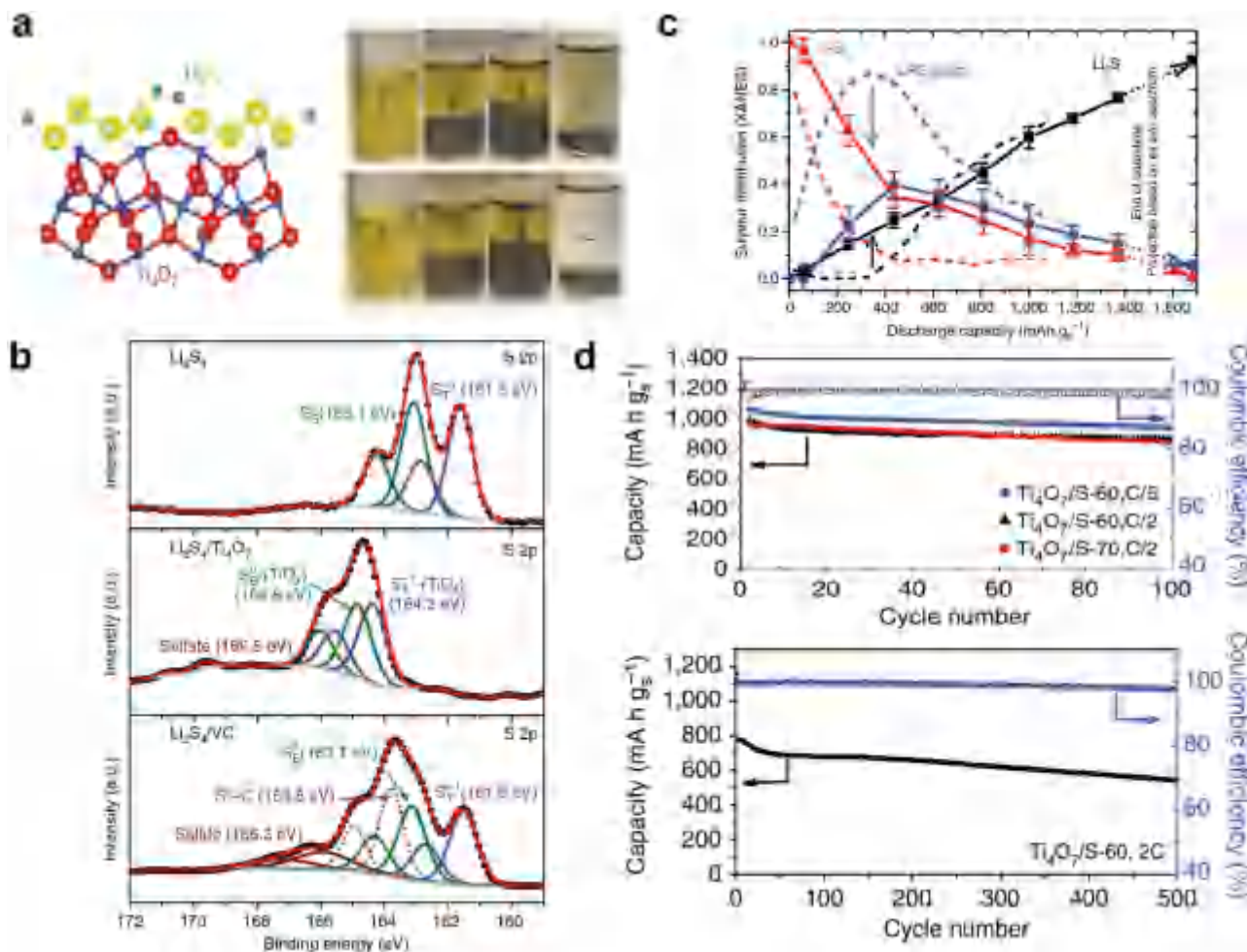


Figure 4. The use of Magnéli titanium oxide for Li-S batteries. a) A scheme showing the electron-density transfer between Li_2S_4 and TiO_x (yellow = S, green = Li, blue = Ti, red = O) (left) and a visual polysulfides-absorption test (right) of Li_2S_4 (in tetrahydrofuran) before and after contact with nothing (1), graphite (2), VC carbon (3), and Ti_4O_7 (4). b) High-resolution XPS data of S 2p spectra of Li_2S_4 , $\text{Li}_2\text{S}_4/\text{VC}$ carbon, and $\text{Li}_2\text{S}_4/\text{Ti}_4\text{O}_7$; c) Operando XANES results of Li-S cells with $\text{Ti}_4\text{O}_7/\text{S-60}$ and VC carbon/S-60 cathodes. d) The electrochemical performance of $\text{Ti}_4\text{O}_7/\text{S}$ electrodes. a-d) Reproduced with permission.^[38] Copyright 2014, Nature Publishing Group.

that can accommodate metal atoms. $\beta\text{-MnO}_2$ is with three-coordinate oxide and octahedral metal centers, while $\delta\text{-MnO}_2$ is a poorly crystallized form of MnO_2 characterized by a two-dimensional layered structure consisting of edge-shared MnO_6 octahedra in which cations and water molecules occupy the interlayer region. MnO_2 is always characteristically nonstoichiometric and is deficient in oxygen atoms.

Using MnO_2 as a host material has been proposed recently. Liang et al.^[63] firstly designed a highly efficient polysulfide mediator monoclinic potassium birnessite $\delta\text{-MnO}_2$ for Li-S batteries. A one-step facile method using GO as the template was applied to fabricate $\delta\text{-MnO}_2$ nanosheets. The as-obtained 75S/ MnO_2 nanocomposite (containing 75% sulfur) cathode displayed an initial capacity of $\approx 1300 \text{ mA h g}^{-1}$ at C/20, 1120 mA h g^{-1} at C/5, and 950 mA h g^{-1} at 1.0C. An in situ visual-electrochemical investigation with 75S/ MnO_2 and a control sample 75S/KB (75% sulfur and 25% Ketjen Black) electrode was conducted. Figure 6b illustrates that the electrolyte in the 75S/KB cell changes from colorless to bright yellow-green on partial discharge of the cell over 4.0 h. At the end of the

discharge (12.0 h), the electrolyte is still yellow, indicating the polysulfides remain in solution. In contrast, in the 75S/ MnO_2 cell, the electrolyte exhibits only a faint yellow color at 4.0 h. On full discharge, the electrolyte is rendered completely colorless. The comparative experiment reveals that MnO_2 is effective in conversion of polysulfides into insoluble reduced species of $\text{Li}_2\text{S}_2/\text{Li}_2\text{S}$. XPS study of the interaction of lithium (poly)sulfides and MnO_2 nanosheets is shown in Figure 6c. Two are terminal and bridging S environments, which are the same as in Li_2S_4 . The S $2p_{3/2}$ peak at 167.2 eV corresponding to the S = O sulfur in thiosulfate ($[\text{SSO}_3]^{2-}$) arises from a surface redox reaction between Li_2S_4 and $\delta\text{-MnO}_2$. The peak at 641.4 eV is from the Mn^{3+} contribution in the Mn $2p_{3/2}$ XPS spectrum and two additional Mn $2p_{3/2}$ peaks arising at lower energy (640.4 and 639.4 eV) are readily attributable to Mn^{2+} . The existence of thiosulfate and the reduction of Mn ions in $\delta\text{-MnO}_2$ confirm the reactions between the polysulfides and the $\delta\text{-MnO}_2$.

$\delta\text{-MnO}_2$ nanosheets can chemically bind polysulfides strongly. However, $\delta\text{-MnO}_2$ nanosheets cannot afford physical confinement of sulfur species. Through construction of hollow

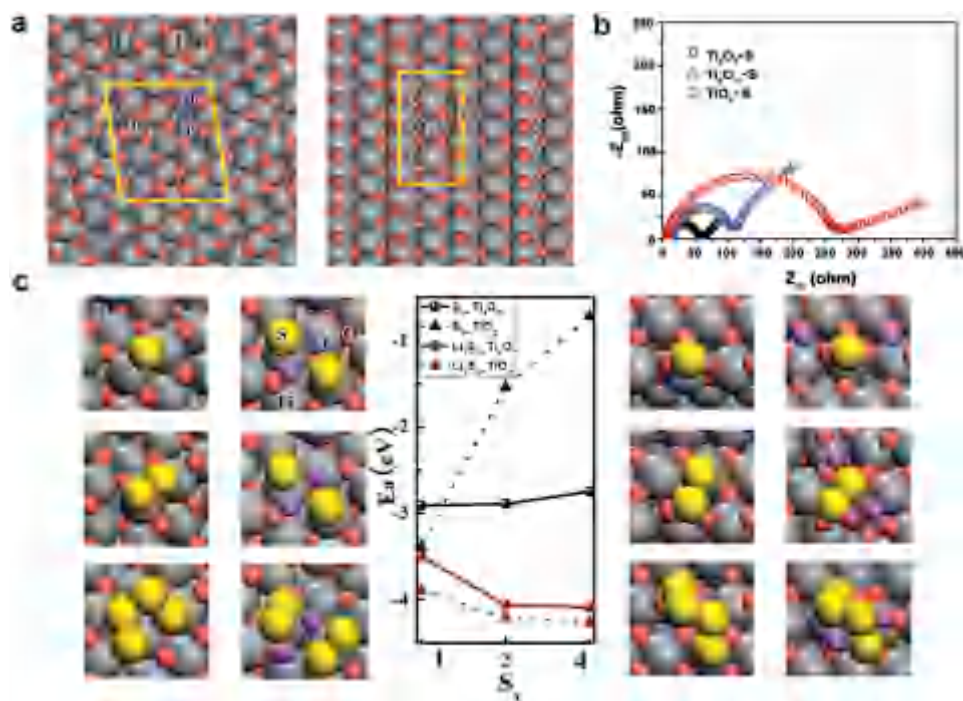


Figure 5. The modeling of polysulfide anchoring on Magnéli titanium oxide. a) Schemes of Magnéli phase Ti_4O_7 (1-20) and the $\beta\text{-TiO}_2$ (110) (gray = Ti, pink = O). b) Nyquist plots of Li-S cells with $\text{Ti}_4\text{O}_7\text{-S}$, $\text{Ti}_6\text{O}_{11}\text{-S}$, and $\text{TiO}_2\text{-S}$ samples. c) DFT analysis of the adsorption of S species on Ti_4O_7 (1-20) and TiO_2 (110) surfaces. a–c) Reproduced with permission.^[39] Copyright 2014, American Chemical Society.

structures, Lou and co-workers pioneeringly designed and fabricated a 1D composite nanoarchitecture, namely hollow carbon nanofibers filled with sodium monoclinic birnessite MnO_2 nanosheets as the host for sulfur.^[62] This provides an efficient sulfur host and 3D interconnected conductive network for cathode structure engineering with both physical confinement and chemical adsorption (Figure 6d). The hollow carbon nanofibers filled with MnO_2 nanosheets ($\text{MnO}_2\text{@HCF}$) have a high specific surface area of approximately $460\text{ m}^2\text{ g}^{-1}$ and hierarchical mesoporous texture. Figure 6e displays nanostructures of $\text{MnO}_2\text{@SiO}_2\text{@C}$, $\text{MnO}_2\text{@HCF}$, and $\text{MnO}_2\text{@HCF/S}$. The cathode material $\text{MnO}_2\text{@HCF/S}$ composite has a sulfur loading of 71 wt%. In order to achieve high energy density, an areal sulfur loading of approximately 3.5 mg cm^{-2} was employed. As shown in Figure 6f, the $\text{MnO}_2\text{@HCF/S}$ composite delivered an initial discharge capacity of 1147 mA h g^{-1} , and more importantly, it was able to maintain a stable cycling performance for 100 charge/discharge cycles at 0.2C. A pure $\text{MnO}_2\text{@HCF}$ composite without sulfur as the cathode of a Li-S cell was tested to confirm that the $\text{MnO}_2\text{@HCF}$ has almost negligible capacity contribution. In the voltage range of 1.7–2.8 V, a capacity of $<10\text{ mA h g}^{-1}$ at 0.1 A g^{-1} was observed, indicating that the $\text{MnO}_2\text{@HCF}$ host has almost no capacity contribution to the Li-S battery.

Very recently, a unique core-shell sulfur- MnO_2 composite with a high sulfur loading up to 85 wt% was proposed by Liang and Nazar.^[64] The thickness of the shell was determined to be $50 \pm 30\text{ nm}$. The birnessite MnO_2 existed in the form of $\text{K}_x\text{MnO}_{2-\delta}$ ($x \approx 0.15$), which has negligible capacity contribution in the voltage window of 1.8–3.0 V (vs Li/Li⁺). A Li-S cell with sublimed sulfur/ MnO_2 composite as the cathode delivered

an initial capacity of 780 mA h g^{-1} and a retained capacity of 480 mA h g^{-1} after 800 cycles at 2.0C, corresponding to a decay rate of 0.048% per cycle. A high sulfur loading of 2.8 and 4.1 mg cm^{-2} can be cycled with more than 600 mA h g^{-1} in 200 cycles at C/5. This is a pioneer study for high sulfur utilization with black semiconductor MnO_2 coating.

Besides the effective adsorption and conversion of polysulfides of $\delta\text{-MnO}_2$, like TiO_2 , different polymorphs of MnO_2 have been investigated in Li-S cells, such as $\alpha\text{-MnO}_2$ nanowires^[65] and ordered mesoporous $\beta\text{-MnO}_2$.^[66] However, the mechanism of the MnO_2 in the sulfur cathodes was not clearly elucidated. The interactions between the polysulfides and MnO_2 with different crystal phases should be further explored by theoretical and experimental investigations. The good combination of intrinsic insulating MnO_2 with conductive scaffolds is strongly required to demonstrate the potential of the oxide for robust use of active sulfur in a working Li-S cell.

2.4. NiFe_2O_4

Spinel is a class of crystals of $\text{A}^{2+}\text{B}^{3+}_2\text{O}_4$ that crystallize in a cubic system with the cations A/B occupying the octahedral and tetrahedral sites and the oxygen anions arranged in a cubic close-packed lattice. As a stable oxide crystal, the use of spinel has also been explored.

Coupled with nanostructured carbon materials, NiFe_2O_4 was recently used as an anode material for lithium-ion batteries.^[67] Wang and co-workers demonstrated a ternary hybrid material consisting of highly conductive CNTs as an electron-conduction framework, nonconductive spinel NiFe_2O_4 as a polysulfide

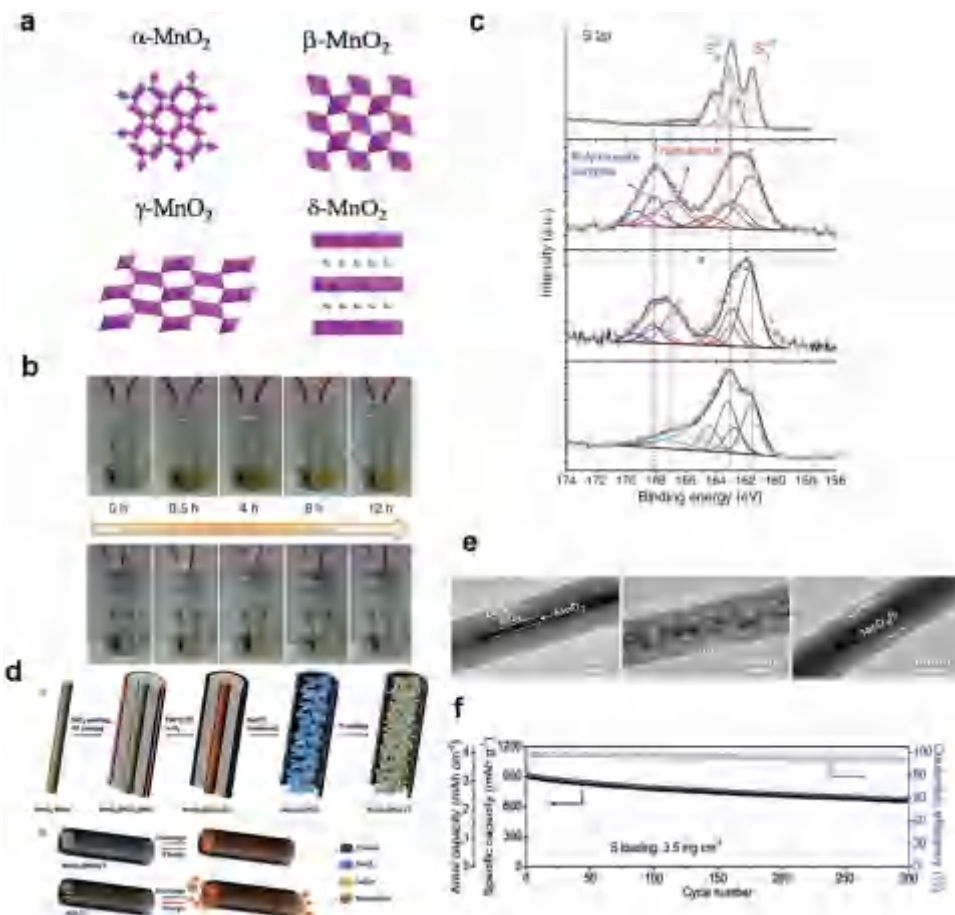


Figure 6. The use of MnO₂ for Li–S batteries. a) The typical polymorphs of MnO₂. b) Visual confirmation of polysulfide entrapment of MnO₂ at specific discharge depths (75S/KB, top; 75S/ MnO₂, down). c) The ex situ XPS of S/MnO₂ electrodes after discharge to specific states: from top to bottom: discharged to 2.15 V, discharged to 2.15 V and then aged in the cell for 20 h, discharged to 800 mA h g⁻¹ and discharged to 1.8 V. d) A synthesis procedure of the MnO₂@HCF/S composite (top) and advantages of the MnO₂@HCF/S composite over HCF/S (bottom). e) TEM images of MnO₂@SiO₂@C, MnO₂@HCF, and MnO₂@HCF/S. f) The prolonged cycling performance of MnO₂@HCF/S at 0.5C and the corresponding Coulombic efficiency. a) Reproduced with permission.^[61] Copyright 2015, Royal Society of Chemistry. b,c) Reproduced with permission.^[60] Copyright 2015, Nature Publishing Group. d–f) Reproduced with permission.^[62] Copyright 2015, Wiley-VCH.

absorber, and sulfur as the electrochemical active material.^[68] The 2D metal oxide nanosheets afford strong binding sites for polysulfides and thus restrict shuttling. At 0.1C, the cell with the CNT/NiFe₂O₄–S ternary material as the cathode exhibited a high reversible specific capacity of 1350 mA h g⁻¹. Reversible specific capacities at different current densities of 0.1, 0.2, 0.5, 1, and 2C were 1350, 1200, 1050, 900, and 700 mA h g⁻¹, respectively. Long-term cycling performance of the ternary material was tested. A specific capacity higher than 850 mA h g⁻¹ was retained after 500 recharging cycles, corresponding to a capacity decay as low as 0.009% per cycle with excellent Coulombic efficiency higher than 99.2%.

Spinel represents a group of oxides with controllable compositions and nanostructures. The insulating nature of spinel requires conductive agents to introduce the electron to the active sites. The combination of spinel with carbon through mixing or in situ carbon deposition has been explored. However, the rational chemical anchoring of polysulfides onto spinel phases has rarely been considered up to now. With the consideration of stability and facile component modulation on spinels,

there is enough space to be explored to recognize the complex interfacial interactions in a working Li–S cell to achieve the best material with the spinel phase for bulk applications.

2.5. Other Oxides as Host Materials for Li–S Batteries

The use of an oxide host for Li–S batteries is also of wide interest. There are some other metal oxides, such as Mg_{0.6}Ni_{0.4}O,^[41,69,70] Mg_{0.8}Cu_{0.2}O,^[71] SiO₂,^[42,72] SiO_x,^[73] Al₂O₃,^[74–77] La₂O₃,^[78] MoO₂,^[79] V₂O₅,^[63,80] V₂O₃,^[63] VO_x,^[73] SnO₂,^[81] CeO₂,^[82] ZrO₂,^[83] Si/SiO₂,^[84] Fe₂O₃,^[85] MgO,^[86] ZnO,^[86,87] Co₃O₄,^[88] have been explored as host materials for Li–S batteries. For example, Mg_{0.6}Ni_{0.4}O was synthesized by the self-propagation high-temperature synthesis method and then it was mixed with polyacrylonitrile; sulfur was infiltrated into the composite through the melt-diffusion method. At different processing conditions, we can achieve diversified ternary sulfur/polyacrylonitrile/Mg_{0.6}Ni_{0.4}O (S/PAN/Mg_{0.6}Ni_{0.4}O) composite.^[70] The cell demonstrated enhanced reversibility, resulting in a discharge

capacity of about 1223 mA h g⁻¹ at the second cycle and it retained almost 100% of this value over 100 cycles. This extraordinary performance is attributed to the addition of Mg_{0.6}Ni_{0.4}O and the formation of the stable structure between sulfur and PAN.^[89] Through employing absorption of the intermediate polysulfides by a porous silica embedded within the carbon-sulfur composite, the initial discharge capacity of the cell with SBA-15 was 960 mA h g⁻¹ and the 40th cycle discharge capacity was 650 mA h g⁻¹ at a current rate of C/5.

Most oxide nanostructures are coupled with conductive polymers or carbon materials to enhance the overall conductivity of the cathode rather than relying on the intrinsic conductivity to attain the best service performances in the Li-S batteries. Al₂O₃ was coated on carbon/sulfur cathode materials through the ALD method,^[75] the casting method,^[74] and the mixing method.^[76] These studies provide new materials for consideration to effectively anchor polysulfides in the cathode of a Li-S battery.

2.6. The Use of Oxides in Separators, Interlayers, and the Anode in a Li-S Cell

The dissolution of polysulfides benefits the high utilization of large sulfur particles and release the volume expansion of the sulfur cathode, and a high electrolyte/sulfur ratio is required. However, too much electrolyte decreases the energy density of a Li-S cell. When a practical cell is assembled, a high areal sulfur loading of more than 6.0 mg cm⁻² and an electrolyte/sulfur ratio of less than 4 are required to attain the energy density of a pouch cell with an energy density larger than 350 W h kg⁻¹.^[90] In this case, the shuttling of polysulfides is stronger in than the coin cell with a low areal sulfur loading of 0.3–2.0 mg cm⁻². In this case, both shuttling of polysulfides and corrosion of the Li-metal anode should be strongly considered at a cell scale to build a safe Li-S cell with high energy density. If the polysulfides can be effectively anchored by oxide and other polar substrates, intermediate diffusion is therefore retarded, and the corrosion of Li metal anode is alleviated. Therefore, anchoring the polysulfides is also very important for anode protection and reducing the amount of electrolyte in a working cell. Novel battery configurations, which have been confirmed as effective measures afterward, are needed to control the shuttling of polysulfides induced by multi-electron conversion reactions.

The introduction of permselective separators and interlayers contributes to an outstanding enhancement in the Li-ion storage performance of a Li-S cell.^[91] The concept of an interlayer to trap soluble polysulfides was firstly proposed by Manthiram's research group and is very important for a practical cell.^[92] The application of a solid electrolyte of Nafion,^[93] graphene oxide,^[94,95] and composite permselective layers^[96,97] in an organic electrolyte was proposed to block the polysulfides and reduce parasitic reactions on the Li anode. Nanostructured oxides can be incorporated into the interlayer/separator to retard the shuttling of polysulfides and enhance the cell with novel configurations.

Attributed to the high Li-ion diffusion rate in V₂O₅, a micrometer-scale V₂O₅ layer on conventional porous separator (Celgard 3401) was created by Li et al. and it served as a separator

that is both lithium-ion-conductive and soluble-polysulfides-impeditive (Figure 7a,b).^[98] The adhesion of a V₂O₅ layer on the polymer separator is reasonable and no delamination was observed at the fractured interface. The discharge capacity of the Li-S cell with a V₂O₅-layer-coated separator is higher than that with a routine porous separator. The V₂O₅ layer reduces the loss of sulfur. In contrast, the charge voltage of the cell without a V₂O₅ layer did not rise above 2.35 V, corroborating the idea that the shuttling factor is strong enough to make the charging process proceed infinitely.^[9] The effective function of the V₂O₅ layer is in mitigating the shuttling of polysulfides. Even though the V₂O₅ layer is effective in alleviating the "shuttling effect" of a Li-S cell, it increases the cell resistance at the same time. The thickness of the barrier layer on the separator needs to be engineered in order to make a compromise between the effective polysulfide shuttling and rapid lithium-ion diffusion.

TiO₂ also significantly contributes as an interlayer employed in Li-S cells. Coupled with graphene, a mesoporous anatase-TiO₂/graphene thin film was coated on porous CNT/sulfur cathodes (PCNTs-S@G/3%T, TiO₂ accounts for 3 wt%).^[99] Figure 7c shows a comparison of the cell configuration with a coated graphene/TiO₂ film in a Li-S cell and a conventional one. The homogeneous TiO₂ is distributed on the interconnected and overlapping graphene sheets, as shown in Figure 7d. A Li-S cell with this kind of hybrid structure was found to deliver specific capacities of 1121, 1050, and 881 mA h g⁻¹ at 0.2, 0.5, and 1.0C, respectively. At 0.5C, an initial specific capacity of 1050 mA h g⁻¹ was obtained and 1040 mA h g⁻¹ was achieved over 300 cycles. Long cycling tests of PCNTs-S@G/3%T show that 630 and 535 mA h g⁻¹ were still achieved at 2.0 and 3.0C after 1000 cycles, respectively (Figure 7e). A binder-free TiO₂-nanowires/graphene hybrid membrane (TiO₂ NW/G) was used in lithium-polysulfide batteries.^[101] Fourier transform infrared (FTIR) spectroscopy testing of the hybrid after cycling in a lithium polysulfide cell showed that a new peak appears at 522 cm⁻¹, which is ascribed to the interaction of LiPSs and TiO₂ forming a S-Ti-O bond. XPS tests revealed that the TiO₂ NW/G-LiPSs electrode has higher binding energy relative to graphene-LiPSs at the terminal/bridging sulfur peaks, which also confirms the strong interactions between the TiO₂ and the LiPSs. Coupled with an activated-carbon/sulfur cathode, needle-shaped TiO₂ with the rutile phase on carbon nanotube paper was used as a polysulfides barrier in Li-S cells.^[102] Peaks at around 163 eV in the XPS spectra correspond to Ti-S bonding. DFT calculations show that the binding energy between the Li₂S₄ and the rutile TiO₂ (110) plane is 2.02 eV, which is in accordance with previous reports discussed above.^[46]

Through simply coating Al₂O₃ powders on routine separators, a high initial capacity of 976 mA h g⁻¹ and a large reversible capacity of 593.4 mA h g⁻¹ after 50 cycles was achieved at 0.2C in a working Li-S cell.^[103] The lithium-ion transference number of the electrolyte in the Al₂O₃-coated separator is 0.93, which indicates that it is difficult for polysulfides to diffuse through the separator. However, a comparative test of super-P-, TiO₂-super-P-, and Al₂O₃-super-P-coated separators used in Li-S cells^[104] illustrates that a uniform coating on the separator is required if metal oxide nanoparticles are employed. Otherwise, cells without oxide-coated separators

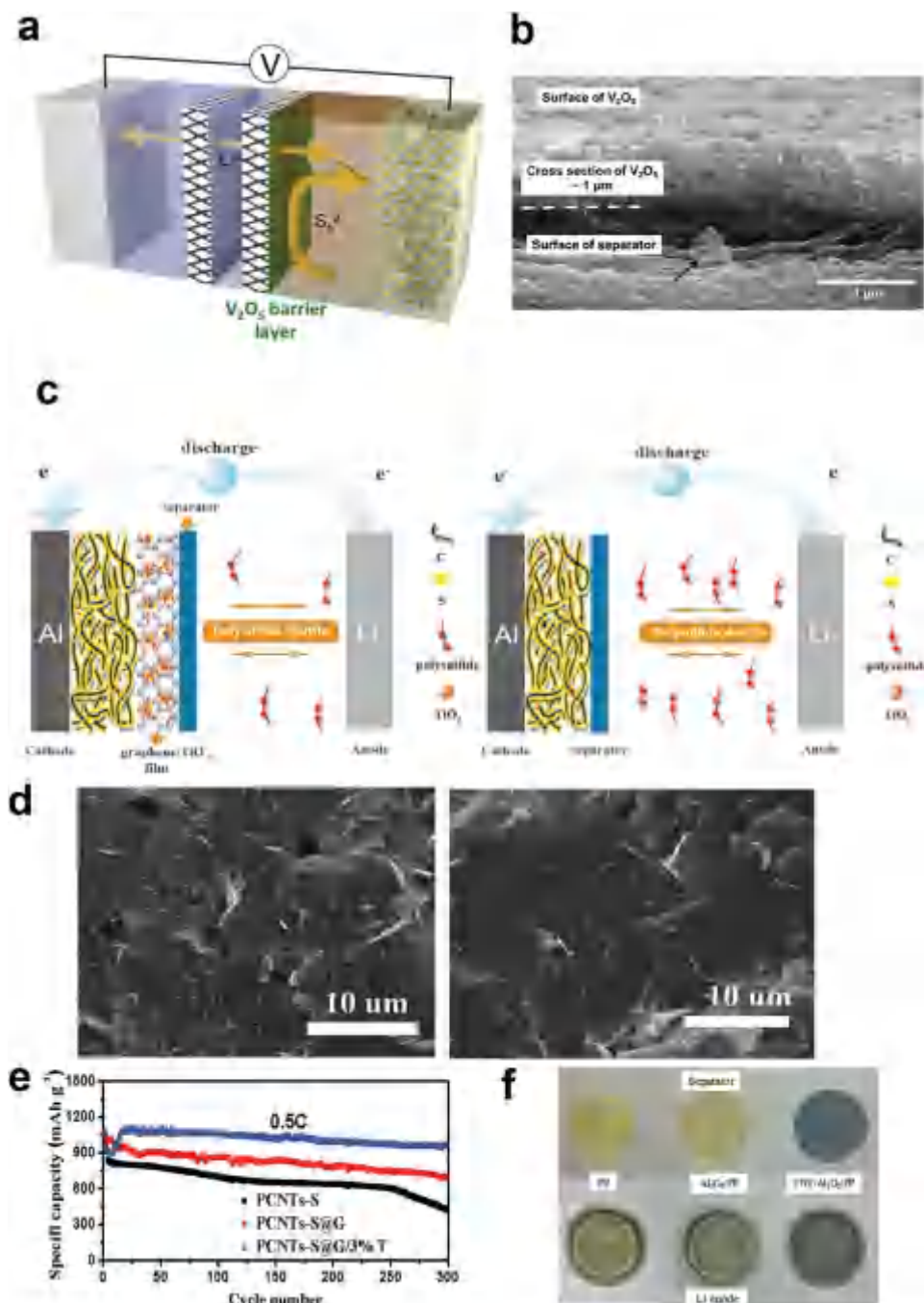


Figure 7. The use of nanostructured oxides as separators for Li-S batteries. a) A schematic of a Li-S battery containing a V₂O₅-coated separator. b) Cross-section SEM of a V₂O₅-coated porous polymeric separator. c) A schematic of the electrode configuration of a Li-S cell with (left) and without (right) a graphene/TiO₂ coated film. d) The front-view SEM image of graphene/TiO₂-coated film (left) and neat graphene-coated film (right). e) The prolonged cycling test of PCNTs-S@G/3%T cathode at 2 and 3C. f) Photographs of separators (close to the lithium side) and lithium electrodes (in the negative can) from the Li-S cells with PP, Al₂O₃/PP, CNT/Al₂O₃/PP after 100 cycles at 0.2C. a,b) Reproduced with permission.^[98] Copyright 2014, American Chemical Society. c-e) Reproduced with permission.^[99] Copyright 2015, Wiley-VCH. f) Reproduced with permission.^[100] Copyright 2015, Springer.

degrade rapidly and fail to display a long cycle life. Micro-sized Al₂O₃ and CNTs were coated in sequence on polypropylene (PP) to make a trilayer separator for Li-S cells.^[100] Initial capacities of batteries with PP, Al₂O₃/PP, and CNT/Al₂O₃/PP separators were 1066, 1233, and 1287 mA h g⁻¹, respectively, at 0.2C. The

cell using CNT/Al₂O₃/PP demonstrated 807.8 mA h g⁻¹ (63% capacity retention) after 100 cycles. Photographs of separators and lithium electrodes after discharge are shown in Figure 7f.

Atomic-layer-deposited Al₂O₃ was coated on an active carbon cloth (Al₂O₃-ACC) and the composite acted as an interlayer in a

Li-S cell.^[105] The cathode was made of a sulfur-infiltrated active carbon cloth, which had a high sulfur loading of 12 mg cm⁻². The surface area of the Al₂O₃-ACC samples was 1692 m² g⁻¹, compared to 1734 m² g⁻¹ for ACC samples. The Al₂O₃-ACC interlayer was found to be more effective in re-collecting and reactivating the polysulfides generated in the discharge of Li-S batteries than an ACC interlayer. An initial specific capacity of 1136 mA h g⁻¹ was obtained for a Li-S cell with an Al₂O₃-ACC layer and 766 mA h g⁻¹ (70%) was achieved after 40 cycles. Moreover, Al₂O₃ is an effective additive in interlayer^[105] and lithium-anode^[106] modifications in Li-S batteries.

Complex inorganic oxides materials (e.g., ceramics,^[107,108] and glass fibers^[109]) were tried to modify separators for Li-S cells. Effective ion separators were demonstrated by coating montmorillonite on the surface of separators.^[108] Glassy fiber^[109] was added between the cathode and microporous separator in a Li-S battery, which delivered more than 500 mA h g⁻¹ (60% retention) even after 500 cycles at a 2C rate. Besides, a glassy separator modified by nonstoichiometric Magnéli phase W₁₈O₄₉ nanowires was used as a polysulfides barrier in Li-S cells.^[110]

When a Li-S cell with high areal sulfur loading was built, not only shuttling of polysulfides, but also anode corrosion and dendrite formation are widely observed to hinder the full demonstration of a Li-S cell with high energy density. Controllable guided deposition of Li ions onto Li metal is a very critical issue. When a Li-metal foil is applied, an unstable solid electrolyte interphase (SEI) is built in an ether-based electrolyte with polysulfides.^[113,111] This induces low utilization of the Li metal with low Coulombic efficiency and continuous decomposition of organic electrolyte. The formation of Li dendrites even induces safety issues. Therefore, the construction of a very stable SEI through the LiNO₃ additive,^[112] LiNO₃-polysulfides,^[113] Cs⁺ salt,^[114] LiI,^[115] LiF,^[116] high-concentration salt,^[117] trimethylsilyl chloride,^[118] and Li₃PO₄ artificial SEI^[114] are applied. The addition of insulating BN^[119] or an amorphous carbon layer^[120] is also effective for protecting the Li anode from continuous corrosion. When a nanostructured conductive scaffold (e.g., Cu nanowires,^[121] Cu foam,^[122] graphene,^[15,123] graphene oxide,^[124] 3D porous carbon matrix with "lithiophilic" coating,^[125] and Li₇B₆ fibers^[126]) was applied, the local current density was significantly decreased and the Li ions preferred to deposit onto the position where the local electrical field was strong. Recently, Archer and co-workers^[127] combined the advantages of a nanostructured solid and a liquid electrolyte by grafting electrolyte molecules into the SiO₂ nanoparticles. The use of SiO₂-containing gel electrolyte that fixes the position of negative charges in the cell and an uneven deposition of Li metal is achieved.

The Li ions were shuttled between the Li-metal anode and the sulfur cathode in a working Li-S cell. The separator provided diffusion channels for controllable transfer of Li ions. The introduction of oxide as a solid electrolyte is another effective route to protecting the Li-metal anode. For instance, when glass fibers (GFs, SiO₂) are introduced as solid electrolytes by Cheng et al.^[128] in a Li metal cell, the GF-based separator is afforded with plenty of polar functional groups between the Li-metal anode and a routine polymer separator (Figure 8a). The polar functional groups of SiO₂ can adsorb considerable numbers of Li ions to compensate the electrostatic interactions and

concentration diffusion between Li ions and protuberances of conventional Cu foil anode, avoiding the accumulation of Li ions around the protuberances. Consequently, dendrite-free Li-metal-based batteries are obtained. Molecular simulation indicated that an elevated binding energy of 3.99 eV is generated between the SiO₂ and the Li, relative to 2.85 eV for Cu and Li. The finite-element method confirmed that the evenly distributed Li ions caused the extra 1.14 eV (Figure 8b,c). After electrochemical tests, Cheng and co-workers discovered that large dendrites with a diameter of 5.0 μm and length of 20–40 μm formed on a conventional Cu foil current collector. In contrast, a dendrite-free morphology was obtained for an anode with GF modification. The dendrite-free morphology led to the enhancement in Coulombic efficiency. Under the current densities of 0.5, 1.0, 2.0, 5.0, and 10.0 mA cm⁻², GF-modified cells were found to deliver enhanced Coulombic efficiencies of 98, 97, 96, 93, and 91%, respectively. When Al₂O₃ particles were applied with graphene in a separator (Figure 8d), a trilayer graphene/PP/Al₂O₃ separator was achieved by Li and co-workers.^[129] Herein, Al₂O₃ enhances the thermal stability and safety of a Li-S battery, since Li metal can be deposited onto the anode uniformly. When an atomic-layer-deposited Al₂O₃ was attached to the lithium anode,^[130] the Al₂O₃ coatings served as protective barriers against corrosion of the Li-metal anode upon air, sulfur, and even organic-solvent exposure (Figure 8e). The first-cycle capacity loss in a working Li-S cell is decreased due to the effective prevention of anode corrosion in the presence of polysulfides. Recently, complex metal oxides such as a membrane based on 3D garnet nanofiber networks^[131] with high lithium-ion conductivity acted as a potential solid electrolyte for Li-S batteries. The surface polarity modification affords an emerging method to inhibit dendrite growth by molecular interactions. The use of polar oxide solid electrolyte efficiently and effectively tunes the Li-ion distribution and evenly distributed Li ions are achieved to inhibit dendrite growth.

Up to now, the modified separator/interlayer system has mainly focused on the blocking of polysulfide shuttling, a rapid transfer pathway for lithium ions, and the effective protection of the lithium metal in a working Li-S cell. The role of the oxide is not fully understood yet. Some metal oxides have very high diffusion rate for Li ions, which is preferred for them to be embedded into the porous polymer matrix to achieve an efficient interlayer/separator for Li-S batteries. There are obvious disadvantages with the introduction of oxide-based interlayers, although it can block polysulfide shuttling. Both charge-transfer resistance and internal resistance are undoubtedly increased when oxide-based interlayers or separators are applied in a working battery. Fortunately, compared to separators, interlayers can reactivate dead sulfur species, which can effectively decrease the internal resistance of the batteries. At the same time, it can contribute to the overall practical capacity at a cell scale.

In summary, nanostructured metal oxides are the most strongly considered inorganic compounds to anchor polysulfides in a complex Li-S battery (Table 1). Nanostructures with abundant interfaces and a tunable exposed surface afford the possibility of significant enhancement in a Li-S cell. These oxides can also be incorporated into the separator/interlayer to

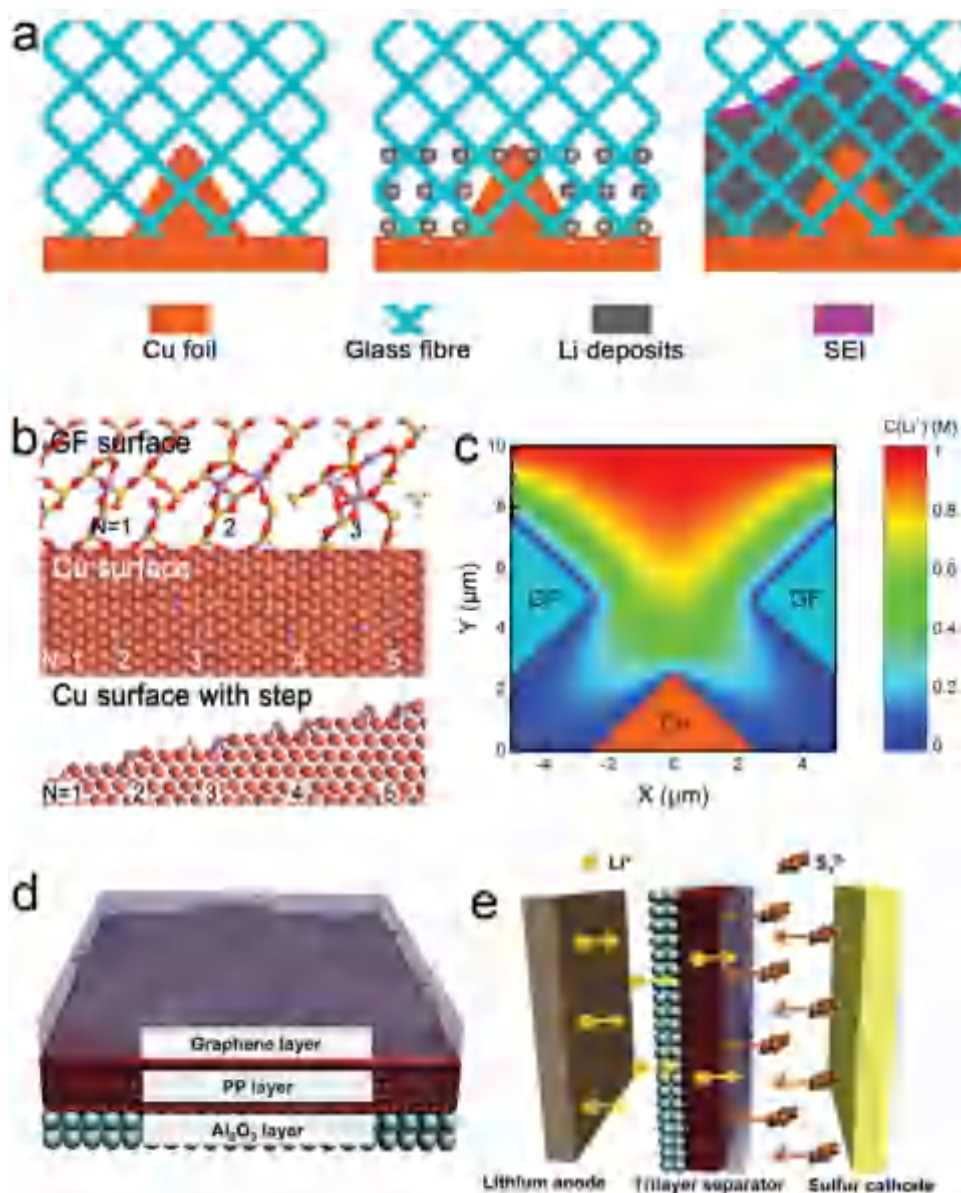


Figure 8. The use of oxide in the separator. a) SiO_2 is with polar Si-O/O-H functional groups introducing a strong interaction with Li ions. The Li ions, by the protuberances on the Cu foil electrode, are evenly redistributed during Li plating and dendrite-free Li deposits are achieved. b) Configurations of Li atoms that bind to SiO_2 fiber, Cu, and Cu substrate with steps. The lithium, oxygen, silicon, and copper atoms are represented by the purple, red, yellow, and orange spheres, respectively. c) The calculated Li^+ distribution on Cu with SiO_2 . d,e) Scheme of the structure of trilayer graphene/polypropylene/ Al_2O_3 separator (d) and its application in a Li-S cell (e). a–c) Reproduced with permission.^[128] Copyright 2016, Wiley-VCH. d,e) Reproduced with permission.^[129] Copyright 2016, Elsevier.

render a cell with a novel configuration. This not only retards the shuttling of polysulfides, but also protects the anodes. However, the exact role of oxides in the Li-S system is not well understood yet. Operando characterization of the phase structure, interfacial chemistry, and the dynamics of metal oxides is highly recommended to provide direct evidence. The modelling and theoretical calculation of oxide-containing Li-S batteries is another effective way to gain new insights of energy chemistry from the scale ranging from the bonding formation to bulk diffusion.

3. Sulfides as Host Materials in Cathodes for Li-S Batteries

Metal sulfides exist widely in nature. Pyrite is the predominant structural type of metal disulfides, which are composed of infinite three-dimensional networks of the metal and discrete S_2^{2-} units. It can be described as a distorted NaCl-type structure in which the rod-shaped S_2^{2-} units are centered on the Cl positions but are oriented so that they are inclined away from the cubic axes.^[136]

Table 1. Different oxides and sulfides employed in cathodes for lithium–sulfur batteries.^{a)}

Polar host material	Synthesis method	Morphology	Sulfur loading & (sulfur content in cathode by weight) [mg cm ⁻²] & [%]	Voltage window (vs. Li ⁺) [V]	Electrochemical performance (initial capacity [mA h g ⁻¹] and cycles) & decay rate claimed (per cycle)	Sulfur infiltration method	Ref.
α -TiO ₂ (anatase)	Sol–gel and soft-template method	Particles (4 wt% in mesoporous carbon)	N/A & (=48%)	1.5–2.8	1201 (73% C ₂₀₀ /C ₁₀) at C/2 & (N/A)	Melt-diffusion	[45]
β -TiO ₂ (rutile)	Commercial product	Particles (4 wt% in mesoporous carbon)	N/A & (=48%)	1.5–2.8	1135 (62% C ₂₀₀ /C ₁₀) at C/2 & (N/A)	Melt-diffusion	[45]
γ -TiO ₂ (brookite)	Sol–gel and annealing method	Particles (4 wt% in mesoporous carbon)	N/A & (=48%)	1.5–2.8	1094 (44% C ₂₀₀ /C ₁₀) at C/2 & (N/A)	Melt-diffusion	[45]
β -TiO ₂ (rutile)	Hydrothermal method	Nanotubes	0.6–1.8 & (=59%)	1.5–3.0	701 (58% after 100 cycles) at C/10 & (N/A)	Melt-diffusion	[39]
TiO ₂ (amorphous)	Sol–gel method	Yolk–shell (with sulfur)	0.4–0.6 & (=53%)	1.7–2.6	1030 (67% after 1000 cycles) at C/2 & (0.033%)	Chemical co-precipitation	[47]
TiO ₂	Atomic layer deposition (ALD)	Ultrathin layer (on nitrogen-doped graphene/sulfur)	1.3–1.8 & (59%)	1.7–2.8	1070 (=86% after 500 cycles) at 1C & (N/A)	Melt-diffusion	[46]
TiO _{2-x} (mixed phases)	Sol–gel, template and annealing	Inverse-opal 3D structure	≈0.8 & (=45%)	1.8–2.6	1098 (81% after 200 cycles) at C/5 & (N/A)	Melt-diffusion	[52]
Ti ₄ O ₇	Hydrothermal, template method and annealing	Particles	0.6–1.8 & (=51%)	1.5–3.0	623 (97% after 250 cycles) at C/2 & (0.012%)	Melt-diffusion	[39]
Ti ₄ O ₇	Sol–gel and annealing	Nanoparticles	1.5–1.8 & (=48%)	1.8–3.0	850 (70% after 500 cycles) at 2C & (0.06%)	Melt-diffusion	[38]
Ti ₆ O ₁₁	Hydrothermal, template method and annealing	Nanowires	0.6–1.8 & (=52%)	1.5–3.0	713 (89% after 100 cycles) at C/10 & (N/A)	Melt-diffusion	[39]
δ -MnO ₂	Chemical co-precipitation	Nanosheets	0.7–1.0 & (=56%)	1.8–3.0	1120 (=92% after 200 cycles) at C/5 & (0.04%)	Melt-diffusion	[132]
δ -MnO ₂	Hydrothermal, template and annealing method	Nanosheets (filled in carbon nanofibers)	3.5–3.9 & (=50%)	1.7–2.8	920 (72% after 300 cycles) at C/2 & (N/A)	Melt-diffusion	[62]
δ -MnO ₂	Chemical co-precipitation	Yolk–shell (microsized)	≈1.5 & (=59%)	1.8–3.0	780 (61.5% after 800 cycles) at 2C & (0.048%)	In situ reaction	[64]
		Yolk–shell (nanosized)	≈1.5 & (=64%)		≈1000 (=31.5% after 1700 cycles) at 2C & (0.039%)		
NiFe ₂ O ₄	Two-step water bath and hydrothermal method	Nanosheets	1.0–1.2 & (=55%)	1.7–2.6	≈900 (nearly no capacity loss after >500 cycles) at 1C & (0.009%)	Chemical co-precipitation	[68]
NiFe ₂ O ₄	Two-step water bath and hydrothermal method	Nanoparticles	1.0–1.2 & (=55%)	1.7–2.6	≈1150 (N/A) at 0.1C (=0.0314%) & (N/A)	Chemical co-precipitation	[68]
Mg _{0.6} Ni _{0.4} O	SHS method	Nanoparticles (4 wt% dispersed in S/PAN composites)	1.0–3.0 & (<61%)	1.0–3.0	1545 (79% after 100 cycles) at 0.1C & (N/A)	Melt-diffusion	[70]
Mg _{0.6} Ni _{0.4} O	Electrospinning	Hollow nanofiber	1.2–1.5 & (=53%)	1.0–3.0	913 (61% after 20 cycles) & (N/A) (calcined at 700 °C)	Melt-diffusion	[69]
La ₂ O ₃	Annealing	Nanoparticles (19 wt% dispersed in mesoporous carbon)	N/A & (48%)	1.5–3.0	1043 (76% after 100 cycles) at 1C & (N/A)	Melt-diffusion	[78]
SiO ₂	Template and annealing method (SBA-15)	Platelets (10 wt% in the sulfur composites)	≈0.72 & (60%)	1.5–3.0	≈980 (66% after 40 cycles) at C/5 & (N/A)	Melt-diffusion	[42]
Al ₂ O ₃	ALD	Ultrathin layer (on S@GO)	≈1 & (<64%)	1.5–2.8	750 (82% after 100 cycles) at C/2 & (N/A)	Chemical co-precipitation	[75]

Table 1. Continued.

Polar host material	Synthesis method	Morphology	Sulfur loading & (sulfur content in cathode by weight) [mg cm ⁻²] & [%]	Voltage window (vs. Li ⁺) [V]	Electrochemical performance (initial capacity [mA h g ⁻¹] and cycles) & decay rate claimed (per cycle)	Sulfur infiltration method	Ref.
Co ₃ O ₄	Hydrothermal and annealing method	Particles (on graphene)	1.2–1.5 & (64%)	1.8–3.0	0.34% decay rate per cycle over 250 cycles & (N/A)	Melt-diffusion	[63]
ZnO	Hydrothermal and annealing method	Laminates	N/A & (60%)	1.0–2.8	1414 (47% after 100 cycles) at C/5 & (N/A)	Melt-diffusion	[87]
ZnO	ALD	Ultrathin layer (on graphene/Sulfur)	1.0–1.2 & (55%)	1.5–2.8	949 (89% after 100 cycles) at C/5 (w/o LiNO ₃) & (N/A)	Chemical co-precipitation	[86]
MgO	ALD	Ultrathin layer (on graphene/Sulfur)	1.0–1.2 & (55%)	1.5–2.8	923 (83% after 100 cycles) at C/5 (w/o LiNO ₃) & (N/A)	Chemical co-precipitation	[86]
V ₂ O ₅	Sol-gel and annealing method	Particles (on graphene)	1.2–1.5 & (64%)	1.8–3.0	≈1000 (76% after 150 cycles) at C/2 & (N/A)	Melt-diffusion	[63]
V ₂ O ₅	Hydrothermal and annealing method	Hollow spheres	1.2–1.5 & (60%)	1.8–2.5	1000 (82% after 300 cycles) at C/5 & (N/A)	Melt-diffusion	[63]
VO ₂	Sol-gel and annealing method	Particles (on graphene)	1.2–1.5 & (64%)	1.8–3.0	≈1000 (74% after 150 cycles; stabilize at ≈400 mA h g ⁻¹ up to 1000 cycles) at C/2 & (N/A)	Melt-diffusion	[63]
MoO ₂	Template and annealing method	Mesoporous particles	≈0.32 & (32%)	1.7–2.8	1100 (62% after 100 cycles and 52% after 250 cycles) at C/10 & (0.19%)	Melt-diffusion	[79]
Co ₉ S ₈	Microwave-assistive solvothermal method	Nanosheets	1.5 (typical) & (60%) 2.5–4.5 & (60%)	1.8–3.0	863 (75% after 400 cycles) at 1C & (N/A) Average 4.3 mA h cm ⁻² for 150 cycles & (N/A)	Melt-diffusion	[133]
CoS ₂	Solvothermal	Microsized particles (15 wt% mixed with graphene)	0.4 & (≈60%) 2.9 & (≈60%)	1.7–2.8	1368 (73% after 150 cycles) at C/2 & (N/A) Average 2.5 mA h cm ⁻² for 30 cycles & (N/A)	Melt-diffusion	[40]
FeS ₂	Commercial	Microsized particles	2.0 ± 0.1 & (62%)	1.7–2.8	1129 (62% after 200 cycles) at C/6.7 & (N/A)	Melt-diffusion	[134]
SnS ₂	Chemical vapor deposition method	5–7 nm nanoparticles (10 wt%) distributed in hollow carbon nanospheres	N/A & (48%)	1.8–3.0	1237.5 (≈75% after 200 cycles) at 0.2C & (N/A)	Wet-impregnation	[135]

^{a)}The electrolyte of tested batteries is made up of 1 M lithium bis(trifluoromethanesulphonyl)imide (LiTFSI) in a 1:1 volume of 1,2-dimethoxyethane (DME):1,3-dioxolane (DOL) with varied amounts of 0–5 wt% LiNO₃ in different articles.

With the enrichment in synthesis methods of two-dimensional dichalcogenides in recent two years, metal sulfides have been explored for Li–S batteries. Metal sulfides have several intrinsic benefits in: i) the strong sulfiphilic property to sulfur-containing species and ii) low lithiation voltages vs Li/Li⁺, which can avoid overlap in the working voltage window of Li–S batteries. Compared to metal oxides, there are a large number of metallic or half-metallic phases of metal chalcogenides, such as pyrite, spinel, and NiAs structures.^[136] Great progress has been made in metal chalcogenides for hydrogen-evolution reactions. With the same demand for nanostructured metal sulfides with high conductivity, many kinds of metal sulfides have swarmed into Li–S batteries. Sulfiphilic cathode materials with strong affinity for lithium (poly)sulfides are a promising new group of

candidates to control dissolution/precipitation reactions in the cell. In this section, the research progress on the use of sulfides as the host material for Li–S batteries is reviewed.

3.1. Co₉S₈

The use of two-dimensional sulfide, TiS₂, nanosheets in a Li₂S cathode^[137] and inspiring computational predictions^[138] promote a wide interest in metal sulfides employed in solid sulfur cathodes. Metal sulfides with high theoretical conductivity are diverse. Co₉S₈ is a member of the Pentlandite family, with a particularly high room-temperature conductivity of 290 S cm⁻¹. A unique graphene-like Co₉S₈ material with interconnected

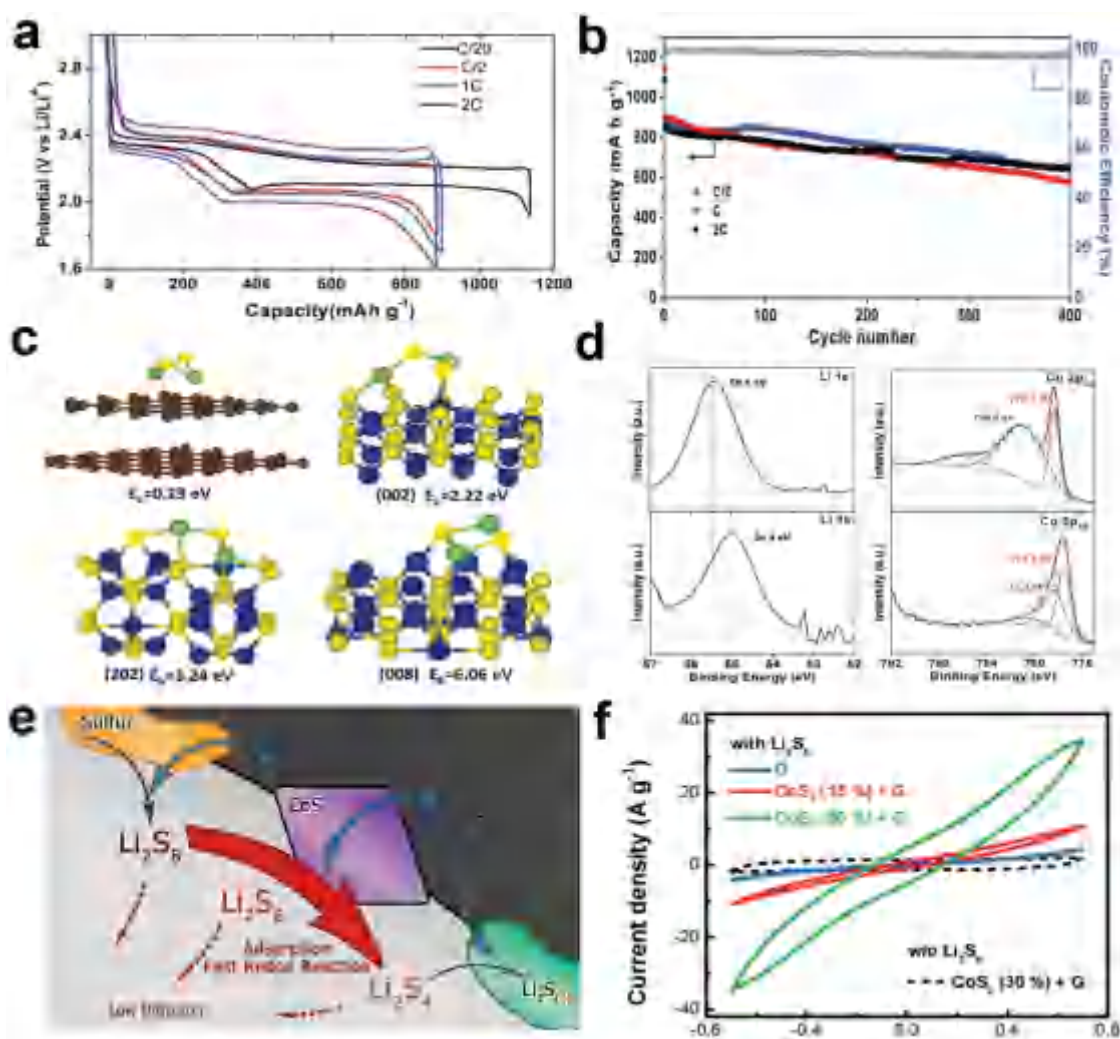


Figure 9. The use of nanostructured sulfides for Li-S batteries. a) The cell voltage profiles of $\text{Co}_9\text{S}_8/\text{S75}$ electrodes at various C rates. b) The prolonged cycling of the discharge capacity retention of $\text{Co}_9\text{S}_8/\text{S75}$ electrodes at C/2, 1C, and 2C rates over 400 cycles. c) DFT calculations of interactions between Li_2S_2 and graphitic carbon, and Co_9S_8 (002), (202) and (008) surface. d) High-resolution XPS spectra of Li 1s and Co $2p_{3/2}$ for Li_2S_4 and Co_9S_8 (top) and after their contact (bottom). e) A schematic illustration of the discharge process in Li-S cell with CoS_2 -incorporated carbon/sulfur cathode. f) Polarization curves of symmetrical Li_2S_6 - Li_2S_6 cells with different electrodes. a-d) Reproduced with permission.^[133] Copyright 2016, Royal Society of Chemistry. e,f) Reproduced with permission.^[40] Copyright 2016, American Chemical Society.

nanosheets that form 3D networks was synthesized through a microwave-assisted solvothermal method by Pang et al.^[133]

The $\text{Co}_9\text{S}_8/\text{S75}$ sulfur composite was prepared via a simple melt-diffusion method at 155 °C for 12 h. The coupled interaction of Co_9S_8 with Li_2S_n relies on $\text{S}_n^{2-}-\text{Co}^{\delta+}$ and $\text{Li}^+-\text{S}^{\delta-}$ (of Co_9S_8) binding. It has a surface area of 108 $\text{m}^2 \text{g}^{-1}$ and a very large pore volume of 1.07 $\text{cm}^3 \text{g}^{-1}$. Illustrated in Figure 9a, high initial discharge capacities of 1130, 890, 895, and 863 mA h g^{-1} were achieved at 0.05, 0.5, 1.0, and 2.0C, respectively. No capacity decrease was observed upon a rate increase from 0.5 to 2.0C (Figure 9b), indicating the highly favorable power capability, owing to the metallic properties of the Co_9S_8 . As shown in Figure 9c, in order to evaluate the contributions of the Co atoms and the S atoms on the surface in binding LiPSs, three representative surfaces (002), (202), and (008), which exhibit different surface Co/S ratios, are chosen. The (002) and (202) surfaces have Co/S ratios of 1:4 and 5:4, respectively. (008) is terminated

entirely with Co atoms. The binding energies of $\text{S}_n^{2-}-\text{Co}^{\delta+}$ and $\text{Li}^+-\text{S}^{\delta-}$ are interesting. In contrast to the previously reported observation of only Li-S (Li-O) binding between Li_2S_x and layered metal sulfide (oxide), herein a strong synergistic binding effect from both the metal and the sulfide ions is witnessed. The binding of Li^+ to the S of Co_9S_8 and the terminal S to Co (if available) completely dominates the interaction between Co_9S_8 and Li_2S_4 , whereas the bridging “neutral” sulfur participates only on the Co-rich surface (008). This binding energy (6.93 eV with van der Waals interactions included) is the highest reported for a Li_2S on a host surface to date. Comparative XPS tests of pristine Co_9S_8 , pristine Li_2S_4 , and Co_9S_8 - Li_2S_4 solid powders reveal that electron transfer from the Li_2S_4 molecules to the Co atoms results in a shift to lower binding energy of the Co $2p_{3/2}$ spectrum, and electron transfer from the Co_9S_8 surface to the Li ions results in 0.5 eV shift to lower binding energy (54.9 eV) of the Li 1s spectrum (Figure 9d). Prolonged

cycling of the electrodes at all rates exhibited almost identical capacity owing to the metallic properties of Co_9S_8 .

3.2. CoS_2

Pyrite CoS_2 has been proven to have high catalytic activity in polysulfide reduction by Song and co-workers.^[139b] The pyrite-type CoS_2 crystal possesses an appreciable conductivity of $6.7 \times 10^3 \text{ S cm}^{-1}$ at 300 K. Yuan et al. reported a kind of sulfiphilic half-metallic pyrite CoS_2 electrocatalyst to power Li–S battery performance by propelling polysulfide redox.^[40] The concept is illustrated in Figure 9e.

In detail, CoS_2 and graphene material were mixed to construct the CoS_2 (15% or 30%) + graphene (named G) materials. The CoS_2 clusters of ca. 1 μm in size are attached to a highly crumpled graphene substrate, forming electron pathways from the conductive framework to the heteropolar CoS_2 surface. As shown in Figure 9f, cyclic voltammetric tests in the voltage range of -0.7 to 0.7 V were performed for symmetrical Li_2S_6 – Li_2S_6 cells. The current density significantly increases by an order of magnitude as the weight ratio of CoS_2 rises from 0 to 30%, demonstrating that CoS_2 –polysulfide interactions not only statically exist but also dynamically accelerate the electrochemical reactions of lithium polysulfides.^[40] EIS testing indicated that R_{ct} (the resistance of charge transfer) was 1202, 436, and 116 Ω for graphene, CoS_2 (15%)+G, and CoS_2 (30%)+G, respectively, indicating that charge transfer at the CoS_2 –polysulfide interface is much more rapid than at the graphene–polysulfide interface, and the redox kinetics of polysulfides in liquid phase ($\text{Li}_2\text{S}_8 \leftrightarrow \text{Li}_2\text{S}_6 \leftrightarrow \text{Li}_2\text{S}_4$) were improved by introducing highly sulfiphilic CoS_2 hosts.^[40] The CoS_2 is an effective electrocatalyst to tune the redox reaction of polysulfides in a working Li–S cell.

At a low sulfur loading (0.4 mg cm^{-2}), for CoS_2 (30%)+G hosts, the initial discharge capacity was 1174 mA h g^{-1} , for CoS_2 (15%)+G hosts, it was 1368 mA h g^{-1} , 62% higher than for a S/G cathode, which means that 82% of the sulfur was utilized. After 150 cycles, 1005 mA h g^{-1} was preserved for the CoS_2 (15%)+G host. Employing a 3D CNT paper, a high areal sulfur loading of 2.9 mg cm^{-2} and a high capacity of 1131 mA h g^{-1} were attained at 0.1C, corresponding to an energy density of 1098 Wh kg^{-1} based on all the components excluding the separator and electrolyte.

Recently, hierarchically porous CoS_2 /carbon paper has been applied as an interlayer for capturing polysulfides through physical absorption and chemical bonding in a working Li–S cell.^[140] The composite CoS_2 /C/S cathode delivers a high initial utilization of 74% at 0.2C and a long cycling life.

3.3. FeS_2

Pyrite FeS_2 (fool's gold) is the most abundant of all sulfur minerals. It does not contain Fe(IV) but is composed of Fe(II) and S_2^{2-} ions in a distorted rock-salt arrangement. Recently, Zhang and Tran^[134] took advantage of commercial FeS_2 powder to investigate pyrite FeS_2 as an efficient adsorbent of lithium polysulfide for improved lithium–sulfur batteries. In-depth Raman characterization has revealed a blueshift in the

absorbance spectrum, which confirms the FeS_2 – Li_2S_n interactions (which may be written as $\text{Li}_2\text{FeS}_{2+n}$) by the S–S covalent bonds. Using a sulfur cathode with a 77 wt% of sulfur content in a sulfur loading of 2.0 mg cm^{-2} , the Li–S cell delivered an initial capacity of 1129 mA h g^{-1} and the second and third cycle discharge capacity were reduced to 940 and 881 mA h g^{-1} respectively in a voltage window of 2.8 – 1.7 V at 0.5 mA cm^{-2} . The FeS_2 was also directly used as cathode materials in an ether electrolyte. It should be noted that FeS_2 is intrinsically semiconductive. Therefore, the conductivity of the FeS_2 should be greatly improved by the introduction of nanocarbon materials, which is similar to other metal oxide electrodes for Li-ion batteries. When the pyrite FeS_2 is applied in an ether electrolyte, the sulfiphilic surface provides abundant anchoring sites for polysulfide intermediates. However, a detailed molecular mechanism for the interactions between the polysulfide and exposed surface of FeS_2 has not been explored yet.

3.4. TiS_2

TiS_2 was the earliest intercalating cathode to be used in secondary lithium batteries.^[17] TiS_2 exhibits a large electronic conductivity and a high diffusion rate of lithium ions. Attributed to its polar surface nature, Archer and co-workers proposed a TiS_2 -supported sulfur cathode.^[141] Different sulfur loadings of 4.6 mg cm^{-2} (TSF5), 21 mg cm^{-2} (TSF10), and 40 mg cm^{-2} (TSF15) within TiS_2 -coated titanium foam delivered initial specific capacities of 20, 25, and 30 mA h cm^{-2} respectively at 2.0 mA cm^{-2} . A capacity of up to $\approx 17 \text{ mA h cm}^{-2}$ can be achieved with a TSF15-based cathode after 100 cycles. It should be noted that no characteristic peak of either Li_2S or LiTiS_2 is observed in the XRD spectra of the discharged electrode, which is attributed to the disturbance of lithium insertion into the structure of Li_2S and LiTiS_2 . This indicates the chemical interaction between LiPSs and TiS_2 . Another study, investigated lithium insertion compounds^[142] such as VO_2 and TiS_2 employed in a sulfur cathode.

The high conductivity and compatibility of TiS_2 with electrolytes means that it is a good candidate in sulfur-cathode materials. However, the mechanistic insights into the nature of polysulfide anchoring onto TiS_2 are not clear yet. The rational design of sulfide/sulfur cathodes can be realized if the interfaces between polysulfides and TiS_2 are more understood.

3.5. Other Sulfides

Various other sulfides have been used as host materials for Li–S batteries, such as MnS ,^[143] CuS ,^[144] ZnS ,^[145] SnS_2 ,^[135,146] NiS_2 ,^[147] and so on. Due to the poor electrical conductivity of sulfides, nanocarbon is always introduced. For instance, a chemical vapor deposition (CVD) method and a wet-impregnation approach was used to synthesize tin-sulfide-anchored sulfur-hollow carbon nanospheres (S/AHCNS– SnS_2).^[135] The S/AHCNS– SnS_2 -10 sample (with 10 wt% SnS_2) delivered an initial capacity of $1237.5 \text{ mA h g}^{-1}$ and retained a capacity of $943.3 \text{ mA h g}^{-1}$ after 200 cycles at 0.2C.

Based on previous research, we have summarized nanostructured metal oxide and sulfide host materials employed in Li–S batteries and they are listed in Table 1. Metal oxides have been strongly considered as polar substrates to anchor polysulfides, while the application of sulfides is still at an early stage. The use of metal oxides and sulfides affords a cell with a high sulfur utilization and a long span life, which is a significant enhancement over C/S cathodes. Both metal oxides and sulfides have a much higher tap density than routine porous carbon, which leads to the possibility of highly packed electrodes for Li–S cells with ultrahigh volumetric energy density.

However, it should be noted that most of the reports on oxide-/sulfide-based cathodes were with an areal sulfur loading of 0.3–1.5 mg cm⁻², which is far less than the requirement of 5.0 mg cm⁻² for practical cells with high energy density of more than 300 W h kg⁻¹.^[90,148] The bulk diffusion quantity of polysulfides and internal resistance in the electrode hinders the effective use of sulfur materials. The good integration of a 3D electrode with long range CNT and graphene current collectors^[101,149] is a promising way to further combine oxide/sulfide cathodes for Li–S cells with high energy density and long cycle life.

Besides metal oxides and sulfides, other promising materials such as metal carbides^[32,150] hydroxides,^[151] and metal-organic frameworks (MOFs)^[152] have been widely researched in Li–S batteries, but these will not be discussed in detail in this review.

4. The Use of Oxides and Sulfides in Related Li–S Systems

As the solid sulfur cathode has come into a blossoming period, many new systems based on multi-electron Li–S redox couples such as Li/PS batteries,^[153–155] and Li₂S-cathode-based Li–S cells,^[137,156] have emerged.

Compared to traditional lithium-ion batteries, a routine porous separator is unable to block the flood of soluble polysulfides, and multifunctional separators^[94,97,104,157] are highly demanded. The fact that the shuttling of polysulfides cannot be avoided, but can be alleviated in Li–S cells, impels us to employ soluble polysulfides in organic solvents directly. Cui and co-workers first proposed a proof-of-concept Li/PS battery.^[155] This concept makes use of lithium as the anode, a high concentration soluble polysulfides dissolved in a mixture of organic solvents as the electrolyte, and conductive host materials as the cathode materials (Figure 10a). For example, Yao et al.^[158] devised a model system for the spatial control of the deposition of S species using the coexistence of polar and nonpolar electrode surfaces by creating a regularly patterned tin-doped indium oxide (ITO) glassy carbon planar electrode, and have found the more effective selective deposition of Li_xS species onto ITO than on glassy carbon (Figure 10b). In order to investigate the effectiveness of the conductive tin-doped indium oxide nanoparticles on adsorbing lithium polysulfides, electrochemical experiments were conducted. The ITO–C hybrid-nanofiber-based electrode delivered reversible specific capacity above 1000 mA h g⁻¹ after 300 cycles at C/5 with a capacity decay of 0.04% per cycle, while

a carbon-nanofiber electrode with the same electrode mass and mass loading of Li₂S₈ exhibited a lower specific capacity of around 700 mA h g⁻¹. Recently, Cui and co-workers also presented a magnetic-field-controlled lithium-polysulfide semi-liquid battery with ferrofluidic properties, employing γ -Fe₂O₃ nanoparticles in the polysulfide electrolyte.^[159]

Impeded by the sluggish developments of lithium anodes, it is not practical for Li–S batteries to be applied on a large scale in a short time period. Lithium sulfide has been selected as the cathode material, and it may work together with other mature anode technologies, such as a nanostructured silicon anode. From this point of view, Seh et al. used Li₂S@TiS₂ nanostructures as a cathode material^[137] and achieved a specific capacity of 503 mA h g⁻¹ at 4.0C (based on Li₂S) and an areal capacity of 3.0 mA h cm⁻² with high mass loading (5.3 mg cm⁻² based on Li₂S) (Figure 10c). They also employed two-dimensional zirconium disulfide (ZrS₂) and vanadium disulfide (VS₂) as further examples to be used in the Li₂S cathode. Li–S cells with Li₂S@TiS₂ and bare Li₂S cathodes were first charged to 3.8 V (vs Li/Li⁺) and then discharged to 1.8 V (vs Li/Li⁺). As shown in Figure 10d, only the underlying carbon substrate could be observed, rather than the pristine particles on the substrate for the bare Li₂S particles on a sample with a carbon-fiber substrate. Irregular-shaped Li₂S particles were formed on the electrode surface rather than the original Li₂S particles at the end of the discharge. However, little change could be observed from after charging and at the end of discharge for the Li₂S@TiS₂ cathode. As illustrated in Figure 10e, ten points at various depths of discharge (DoD) and states of charge were chosen to probe the sulfur content in the organic electrolyte. The percentage of total sulfur loss in the electrolyte of the Li₂S@TiS₂ cathode (<20% at all ten points) is much less than that for the bare Li₂S cathode (up to 91% at point 3) at all chosen points.

5. General Principle for Rational Design of Polar Substrates for Li–S Batteries

Both metal oxides and sulfides are typical polar substrates to effectively host sulfur and anchor polysulfides in a Li–S cell. However, there are thousands of metal oxides and sulfides with quite different nanostructures and exposed surfaces for electrochemical conversion chemistry of the Li–S system. A general understanding of the rational design of the oxide/sulfide host is strongly required.

Within the complex electrochemical reaction, the interactions between the metal oxides/sulfides and polysulfides are the most important factor. For example, TiO₂ is the most frequently used material in Li–S cells. XPS, FTIR, and Raman spectroscopy tests of the TiO₂ sample, after interaction with polysulfides, have been applied. They are effective tools to probe the formation of Ti–S bonding. Moreover, the visualizing of host materials–Li₂S₄ before and after contact is a vivid way to confirm the interactions between metal oxides/sulfides and polysulfides. The electrochemical titration of S_n²⁻ is an efficient way to vary the capability to absorb polysulfides of various materials.^[133,160]

DFT calculations can give hints on the strength of bonding between hosts and Li₂S_x (1 ≤ x ≤ 8).^[31,161] The DFT method has been widely applied to probe the complex interactions between

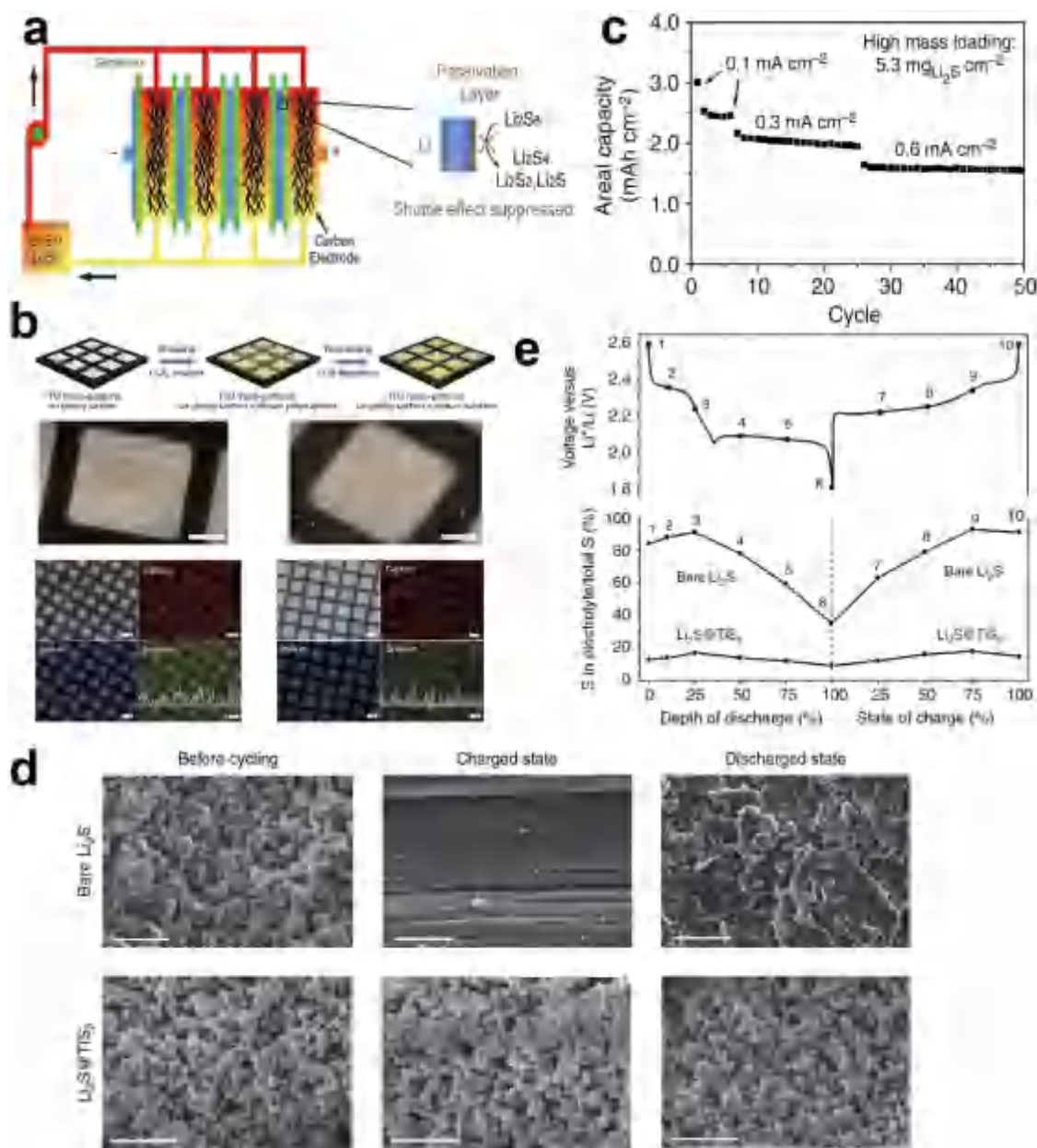
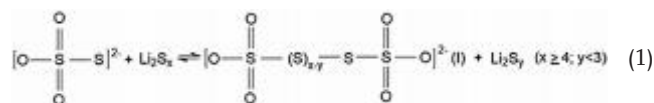


Figure 10. The use of oxides and sulfides in Li/PS battery. a) A schematic illustrating the structure of the Li/PS battery (left) and the magnified scheme (right) showing the SEI passivation layer on lithium with high resistance toward the internal reaction between PS and lithium due to the presence of LiNO₃. b) A demonstration of selective deposition of Li₂S on ITO relative to glassy carbon. c) Typical discharge-charge voltage profile at various DoD and SoC and the corresponding percentage of sulfur in the electrolyte relative to total sulfur mass on the electrode for Li₂S@TiS₂ and bare Li₂S cathodes. d) SEM images of bare Li₂S (top) and Li₂S@TiS₂ (bottom) at electrochemical states. e) Electrochemical performance of Li₂S@TiS₂ cathodes with high mass loading. a) Reproduced with permission.^[155] Copyright 2013, Royal Society of Chemistry. b) Reproduced with permission.^[153] Copyright 2014, Nature Publishing Group. c–e) Reproduced with permission.^[137] Copyright 2014, Nature Publishing Group.

the polysulfides and oxides. For instance, Nazar and co-workers reported that MnO₂ has catalytic power in the conversion of polysulfides, through the combination of theoretical calculation and XPS analysis.^[132] Two proposed reactions are listed below. Polysulfides catenate to the thiosulfate by inserting into the S–S single bond to create a polythionate complex (I) and short-chain polysulfide (i.e., Li₂S₂ or Li₂S) (Reaction (1)) through an internal disproportionation reaction. Only one –SO₃ group can

be formed in the polythionate complex (Reaction (2)). However, the bi-polythionate complex (I) is preferentially generated due to its known stability in aqueous media.



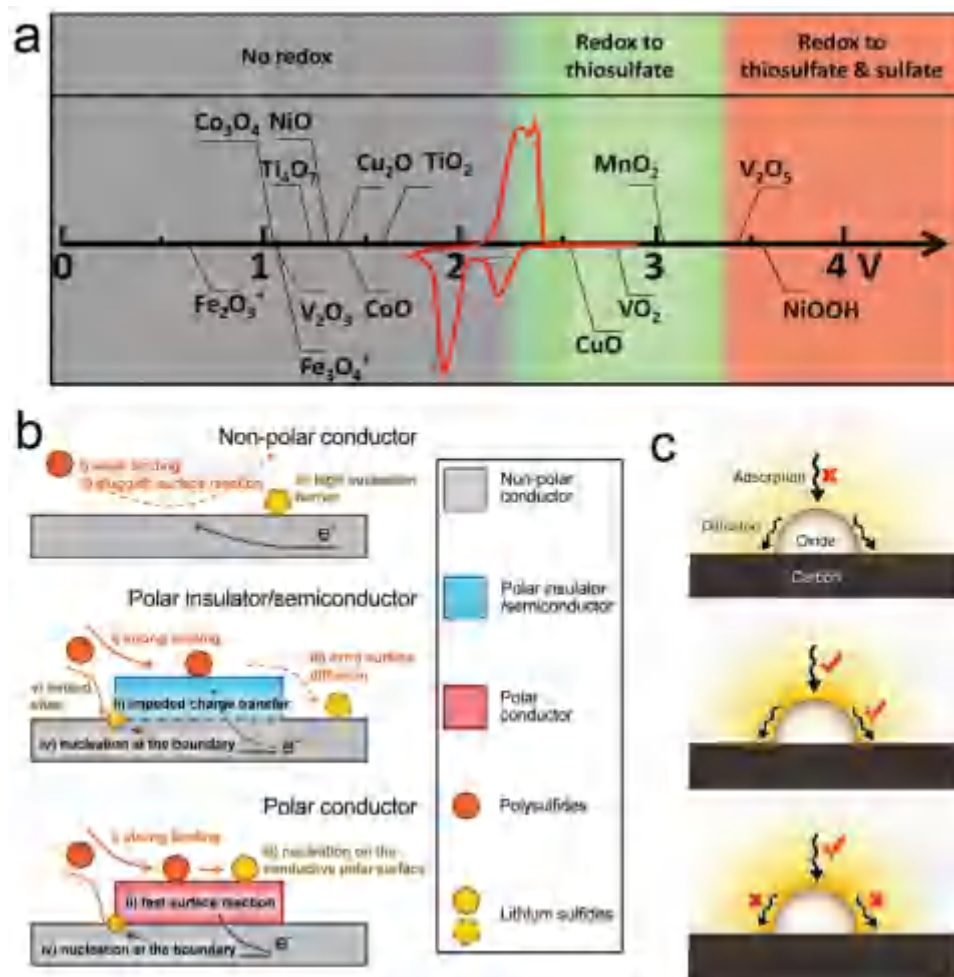
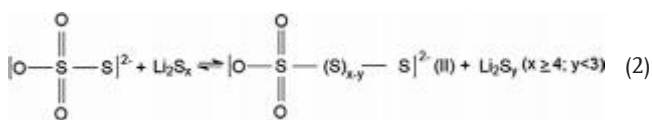


Figure 11. The principle for polar substrate design for Li-S batteries. a) The relationship between the chemical reactivity of different metal oxides with polysulfides and the redox potential vs Li/Li⁺; b) The working mechanism of polar conductor as it meets the request for both charge transferring and adequate binding. c) Scheme of polysulfide adsorption and diffusion on the surface of various insulating metal oxides. a) Reproduced with permission.^[63] Copyright 2016, Wiley-VCH. b) Reproduced with permission.^[37] Copyright 2016, Wiley-VCH. c) Reproduced with permission.^[162] Copyright 2016, Nature Publishing Group.



A “Goldilocks” principle after testing a series of oxides was proposed by Nazar and co-workers to search the best metal oxides (Figure 11a).^[63] The metal oxides are divided into three classes in terms of their redox potential versus Li/Li⁺. Materials with a moderate voltage (vs Li/Li⁺), which form surface-bound thiosulfate via redox, are the most suitable for the cathode host of Li-S cells. δ-MnO₂ is one of these. The conductivity of the material determines the kinetics of electron transfer, which significantly influences the extent of the final conversion of sulfur to Li₂S.

A family of oxides and sulfides affords active sites to strongly anchor polysulfides within the cathode. If the anchoring sites are with superb intrinsic electrical conductivity, the absorbed polysulfides can receive electrons, which facilitates the redox

reaction of the polysulfides (Figure 11b).^[37] Therefore, an ideal polar substrate is expected to be conductive, which facilitates both the liquid-liquid transformation of the polysulfides and the liquid-solid nucleation/growth of the Li₂S. Some polar substrates (e.g., CoS₂)^[40] can even serve as an electrocatalyst to reduce the overpotential of the polysulfide redox reaction and improve the utilization of the sulfur cathode. However, an electrocatalyst to enhance the redox reaction between Li₂S and Li₂S₂ is currently still lacking.

If we consider the poor conductivity of most metal oxides, the absorbed polysulfides should be transferred from the surface to the conductive substrate to undergo the electrochemical reaction. According to pioneering work carried out by Tao et al., the balance optimization between polysulfide adsorption and diffusion on the surface of the metal oxides is necessary (Figure 11c).^[162] Composite cathode materials based on the MgO, CeO₂, and La₂O₃ exhibited high discharge capacity and excellent cycling performance. If one intends to select an oxide and other insulating polar substrate, polar hosts with strong

binding with polysulfides, high surface area, and extraordinary surface diffusion properties are preferred.

Besides, nanostructures play an important role in the properties of materials. For instance, surface area, pore distribution, and pore volume are highly dependent on the nanostructures of metal oxides and sulfides, which also regulates the adsorption capability of polysulfides. It is interesting that Li_2S is likely to deposit on the edges of MoS_2 rather the terraces.^[163] The size of a catalyst has a substantial impact on its performance. Metal oxides and sulfides with smaller sizes, even down to the scale of quantum dots, may have much better capability in Li–S cells compared to present materials above. There is plenty of room for research on the interaction mechanism between nanostructured metal oxides and sulfides and Li_2S_x ($1 \leq x \leq 8$) in Li–S cells.

6. Conclusions and Perspectives

Recent advances in the use of nanostructured oxides and sulfides or their composites as host materials for advanced Li–S batteries are reviewed here. Several factors influencing the relationships between the properties of the materials and the performance of lithium–sulfur batteries are concluded: i) the adsorption ability to polysulfides; ii) the conductivity of the intrinsic materials or the composites; iii) the catalytic capability in contributing to the mutual conversions of lithium polysulfides (Li_2S_x ($4 \leq x \leq 8$)) and lithium (di)sulfides; iv) the nanostructures that determine the surface area, the 3D morphologies, and the exposure of active sites. Both nanostructured oxides and sulfides have demonstrated outstanding ability to render a composite cathode with high sulfur utilization and long cycle life.

However, selecting the best one among many probable suitable materials is also a grand challenge of Li–S batteries. New characterization methods can speed up this process and save a lot of time and cost compared to routine trial and error methods. Moreover, theoretical approaches are highly required to search, predict, and guide the future developments of Li–S batteries.^[138,164] From the first-principles theory aspect, the binding energy between the host material (or anchoring material) and lithium polysulfides or lithium (di)sulfides plays a critical role, and the partial density of states near Fermi energy level is an indicator of the theoretical conductivity of a material. At the same time, it follows the trends of the materials genome initiative.^[165]

Toward the practical applications of Li–S batteries, abundant factors should be carefully considered to provide a holistic solution. Besides these cutting-edge matters, some old obstacles, such as the low areal sulfur loading amounts, large electrolyte volume/sulfur ratio, and subsequent low volumetric energy density, should be overcome gradually. Areal loadings of sulfur in cathodes with nanostructured metal oxides or sulfides as additives are mostly in between 0.3 and 2 mg cm^{-2} . There is a long way to go in a high-sulfur-loading cathode with oxide or sulfide additives. Nanostructure engineering or conductive carbon recombination may be a rational solution. The former can sometimes alleviate the volume change.

The polysulfide dissolution and subsequent shuttling problem are highly related to the electrolyte. Sulfur redox-based flow batteries have been developed by taking advantage of the critical disadvantages of the solid-state sulfur cathode. Non-solvent room-temperature ionic liquids are expected to serve as a compromise solution, for the reason that ionic liquids can suppress the solubility of polysulfides while having low Li^+ -ion diffusion coefficients. In the future, regarding cathode research, great attention must be paid to the conversion mechanism of soluble polysulfides and insoluble (di)sulfides on different host materials including pristine/doped carbon, and conductive polymers, as well as 3D inorganic compounds. Some of them may afford an electrocatalytic effect to mediate the redox reaction of the polysulfides. Also, the solid-state conversion of Li_2S_2 to Li_2S should be highly considered, since the redox between Li_2S_2 and Li_2S contributes a high theoretical specific capacity of Li–S batteries if the Li_2S is produced all through the Li_2S_2 . It is expected that the achievements in Li–S batteries will have guidance in other related areas, such as Li–Se batteries, sulfur/polysulfides redox chemistries, and so on.

Acknowledgements

The authors thank the support from National Key Research and Development Program of China (Nos. 2016YFA0202500 and 2016YFA0202603). X.L. and L.M. thank to the National Key Research and development Program of China (2016YFA0202603), the National Basic Research Program of China (2013CB934103), the Program of Introducing Talents of Discipline to Universities (B17034), the National Natural Science Foundation of China (51521001, 51272197), the National Natural Science Fund for Distinguished Young Scholars (51425204) and the Fundamental Research Funds for the Central Universities (WUT: 2015-PY-2, 201611001). X.L., J.Q.H., and Q.Z. give thanks to the Natural Scientific Foundation of China (No. 21306103, 21422604, and 21676160). Q.Z. thanks to the Royal Society for the award of a Newton Advanced Fellowship (Ref: NA140249). The authors thank helpful discussion on this topic from Hong-Jie Peng, Xin-Bing Cheng, Ze-Wen Zhang, and Ge Zhang at Tsinghua University.

Received: April 1, 2016

Revised: September 22, 2016

Published online:

- [1] a) D. Larcher, J. M. Tarascon, *Nat. Chem.* **2015**, *7*, 19; b) P. G. Bruce, S. A. Freunberger, L. J. Hardwick, J. M. Tarascon, *Nat. Mater.* **2012**, *11*, 19; c) S. Evers, L. F. Nazar, *Acc. Chem. Res.* **2013**, *46*, 1135.
- [2] a) A. Manthiram, Y. Z. Fu, S. H. Chung, C. X. Zu, Y. S. Su, *Chem. Rev.* **2014**, *114*, 11751; b) L. F. Nazar, M. Cuisinier, Q. Pang, *MRS Bull.* **2014**, *39*, 436.
- [3] Y. Yang, G. Y. Zheng, Y. Cui, *Chem. Soc. Rev.* **2013**, *42*, 3018.
- [4] a) J. R. Croy, A. Abouimrane, Z. Zhang, *MRS Bull.* **2014**, *39*, 407; b) A. Manthiram, S. H. Chung, C. X. Zu, *Adv. Mater.* **2015**, *27*, 1980; c) J. Liang, Z.-H. Sun, F. Li, H.-M. Cheng, *Energy Storage Mater.* **2016**, *2*, 76; d) A. Rosenman, E. Markevich, G. Salitra, D. Aurbach, A. Garsuch, F. F. Chesneau, *Adv. Energy Mater.* **2015**, *5*, 1500212.
- [5] R. Xu, J. Lu, K. Amine, *Adv. Energy Mater.* **2015**, *5*, 1500408.
- [6] S. S. Zhang, *J. Power Sources* **2013**, *231*, 153.

- [7] M. Wild, L. O'Neill, T. Zhang, R. Purkayastha, G. Minton, M. Marinescu, G. J. Offer, *Energy Environ. Sci.* **2015**, *8*, 3477.
- [8] a) M. Cuisinier, P. E. Cabelguen, S. Evers, G. He, M. Kolbeck, A. Garsuch, T. Bolin, M. Balasubramanian, L. F. Nazar, *J. Phys. Chem. Lett.* **2013**, *4*, 3227; b) C. Barchasz, F. Molton, C. Duboc, J. C. Lepretre, S. Patoux, F. Alloin, *Anal. Chem.* **2012**, *84*, 3973; c) Y. C. Lu, Q. He, H. A. Gasteiger, *J. Phys. Chem. C* **2014**, *118*, 5733; d) J. Nelson, S. Misra, Y. Yang, A. Jackson, Y. J. Liu, H. L. Wang, H. J. Dai, J. C. Andrews, Y. Cui, M. F. Toney, *J. Am. Chem. Soc.* **2012**, *134*, 6337.
- [9] Y. V. Mikhaylik, J. R. Akridge, *J. Electrochem. Soc.* **2004**, *151*, A1969.
- [10] K. Kumaresan, Y. Mikhaylik, R. E. White, *J. Electrochem. Soc.* **2008**, *155*, A576.
- [11] D. W. Wang, Q. C. Zeng, G. M. Zhou, L. C. Yin, F. Li, H. M. Cheng, I. R. Gentle, G. Q. M. Lu, *J. Mater. Chem. A* **2013**, *1*, 9382.
- [12] X. B. Li, P. Guo, T. F. Cao, H. Liu, W. M. Lau, L. M. Liu, *Sci. Rep.* **2015**, *5*, 10848.
- [13] X.-B. Cheng, R. Zhang, C.-Z. Zhao, F. Wei, J.-G. Zhang, Q. Zhang, *Adv. Sci.* **2016**, *3*, 1500213.
- [14] N.-W. Li, Y.-X. Yin, C.-P. Yang, Y.-G. Guo, *Adv. Mater.* **2016**, *28*, 1853.
- [15] R. Zhang, X.-B. Cheng, C.-Z. Zhao, H.-J. Peng, J.-L. Shi, J.-Q. Huang, J. Wang, F. Wei, Q. Zhang, *Adv. Mater.* **2016**, *28*, 2155.
- [16] a) L. Q. Mai, X. C. Tian, X. Xu, L. Chang, L. Xu, *Chem. Rev.* **2014**, *114*, 11828; b) Y. L. Zhao, J. G. Feng, X. Liu, F. C. Wang, L. F. Wang, C. W. Shi, L. Huang, X. Feng, X. Y. Chen, L. Xu, M. Y. Yan, Q. J. Zhang, X. D. Bai, H. A. Wu, L. Q. Mai, *Nat. Commun.* **2014**, *5*, 4565.
- [17] X.-Y. Yu, L. Yu, X. W. Lou, *Adv. Energy Mater.* **2016**, *6*, 1501333.
- [18] a) B. Zhang, X. Qin, G. R. Li, X. P. Gao, *Energy Environ. Sci.* **2010**, *3*, 1531; b) H. B. Wu, S. Y. Wei, L. Zhang, R. Xu, H. H. Hng, X. W. Lou, *Chem.-Eur. J.* **2013**, *19*, 10804; c) G. L. Xu, Y. F. Xu, J. C. Fang, X. X. Peng, F. Fu, L. Huang, J. T. Li, S. G. Sun, *ACS Appl. Mater. Interfaces* **2013**, *5*, 10782.
- [19] a) X. L. Ji, K. T. Lee, L. F. Nazar, *Nat. Mater.* **2009**, *8*, 500; b) D. Li, F. Han, S. Wang, F. Cheng, Q. Sun, W. C. Li, *ACS Appl. Mater. Interfaces* **2013**, *5*, 2208.
- [20] K. Zhang, Q. Zhao, Z. L. Tao, J. Chen, *Nano Res.* **2013**, *6*, 38.
- [21] a) G. Y. Zheng, Q. F. Zhang, J. J. Cha, Y. Yang, W. Y. Li, Z. W. Seh, Y. Cui, *Nano Lett.* **2013**, *13*, 1265; b) G. Y. Zheng, Y. Yang, J. J. Cha, S. S. Hong, Y. Cui, *Nano Lett.* **2011**, *11*, 4462.
- [22] C. F. Zhang, H. B. Wu, C. Z. Yuan, Z. P. Guo, X. W. Lou, *Angew. Chem., Int. Ed.* **2012**, *51*, 9592.
- [23] a) L. X. Yuan, H. P. Yuan, X. P. Qiu, L. Q. Chen, W. T. Zhu, *J. Power Sources* **2009**, *189*, 1141; b) M. Q. Zhao, H. J. Peng, G. L. Tian, Q. Zhang, J. Q. Huang, X. B. Cheng, C. Tang, F. Wei, *Adv. Mater.* **2014**, *26*, 7051.
- [24] a) M. Q. Zhao, Q. Zhang, J. Q. Huang, G. L. Tian, J. Q. Nie, H. J. Peng, F. Wei, *Nat. Commun.* **2014**, *5*, 3410; b) T. Q. Lin, Y. F. Tang, Y. M. Wang, H. Bi, Z. Q. Liu, F. Q. Huang, X. M. Xie, M. H. Jiang, *Energy Environ. Sci.* **2013**, *6*, 1283; c) J. L. Shi, C. Tang, H. J. Peng, L. Zhu, X. B. Cheng, J. Q. Huang, W. C. Zhu, Q. Zhang, *Small* **2015**, *11*, 5243; d) L. F. Fei, X. G. Li, W. T. Bi, Z. W. Zhuo, W. F. Wei, L. Sun, W. Lu, X. J. Wu, K. Y. Xie, C. Z. Wu, H. L. W. Chan, Y. Wang, *Adv. Mater.* **2015**, *27*, 5936.
- [25] a) J. X. Song, M. L. Gordin, T. Xu, S. R. Chen, Z. X. Yu, H. Sohn, J. Lu, Y. Ren, Y. H. Duan, D. H. Wang, *Angew. Chem., Int. Ed.* **2015**, *54*, 4325; b) H. J. Peng, J. Q. Huang, M. Q. Zhao, Q. Zhang, X. B. Cheng, X. Y. Liu, W. Z. Qian, F. Wei, *Adv. Funct. Mater.* **2014**, *24*, 2772; c) M. Q. Zhao, X. F. Liu, Q. Zhang, G. L. Tian, J. Q. Huang, W. C. Zhu, F. Wei, *ACS Nano* **2012**, *6*, 10759.
- [26] a) M. Yu, R. Li, M. Wu, G. Shi, *Energy Storage Mater.* **2015**, *1*, 51; b) J. G. Wang, K. Y. Xie, B. Q. Wei, *Nano Energy* **2015**, *15*, 413; c) M. R. Wang, H. Z. Zhang, Q. Wang, C. Qu, X. F. Li, H. M. Zhang, *ACS Appl. Mater. Interfaces* **2015**, *7*, 3590; d) C. Tang, B. Q. Li, Q. Zhang, L. Zhu, H. F. Wang, J. L. Shi, F. Wei, *Adv. Funct. Mater.* **2016**, *26*, 577; e) L. Y. Chai, J. X. Wang, H. Y. Wang, L. Y. Zhang, W. T. Yu, L. Q. Mai, *Nano Energy* **2015**, *17*, 224.
- [27] a) M. Liu, F. Ye, W. Li, H. Li, Y. Zhang, *Nano Res.* **2016**, *9*, 94; b) H. J. Peng, Q. Zhang, *Angew. Chem., Int. Ed.* **2015**, *54*, 11018; c) G. M. Zhou, E. Paek, G. S. Hwang, A. Manthiram, *Nat. Commun.* **2015**, *6*, 7760.
- [28] a) H. L. Wang, Y. Yang, Y. Y. Liang, J. T. Robinson, Y. G. Li, A. Jackson, Y. Cui, H. J. Dai, *Nano Lett.* **2011**, *11*, 2644; b) L. W. Ji, M. M. Rao, H. M. Zheng, L. Zhang, Y. C. Li, W. H. Duan, J. H. Guo, E. J. Cairns, Y. G. Zhang, *J. Am. Chem. Soc.* **2011**, *133*, 18522; c) W. D. Zhou, H. Chen, Y. C. Yu, D. L. Wang, Z. M. Cui, F. J. DiSalvo, H. D. Abruna, *ACS Nano* **2013**, *7*, 8801.
- [29] a) Y. L. Ding, P. Kopold, K. Hahn, P. A. van Aken, J. Maier, Y. Yu, *Adv. Funct. Mater.* **2016**, *26*, 1112; b) Z. Y. Wang, Y. F. Dong, H. J. Li, Z. B. Zhao, H. B. Wu, C. Hao, S. H. Liu, J. S. Qiu, X. W. Lou, *Nat. Commun.* **2014**, *5*, 5002; c) C. Tang, Q. Zhang, M. Q. Zhao, J. Q. Huang, X. B. Cheng, G. L. Tian, H. J. Peng, F. Wei, *Adv. Mater.* **2014**, *26*, 6100.
- [30] H. J. Peng, T. Z. Hou, Q. Zhang, J. Q. Huang, X. B. Cheng, M. Q. Guo, Z. Yuan, L. Y. He, F. Wei, *Adv. Mater. Interfaces* **2014**, *1*, 1400227.
- [31] J. X. Song, T. Xu, M. L. Gordin, P. Y. Zhu, D. P. Lv, Y. B. Jiang, Y. S. Chen, Y. H. Duan, D. H. Wang, *Adv. Funct. Mater.* **2014**, *24*, 1243.
- [32] Q. Pang, J. T. Tang, H. Huang, X. Liang, C. Hart, K. C. Tam, L. F. Nazar, *Adv. Mater.* **2015**, *27*, 6021.
- [33] C. P. Yang, Y. X. Yin, H. Ye, K. C. Jiang, J. Zhang, Y. G. Guo, *ACS Appl. Mater. Interfaces* **2014**, *6*, 8789.
- [34] G. M. Zhou, L. C. Yin, D. W. Wang, L. Li, S. F. Pei, I. R. Gentle, F. Li, H. M. Cheng, *ACS Nano* **2013**, *7*, 5367.
- [35] X. X. Gu, C. J. Tong, C. Lai, J. X. Qiu, X. X. Huang, W. L. Yang, B. Wen, L. M. Liu, Y. L. Hou, S. Q. Zhang, *J. Mater. Chem. A* **2015**, *3*, 16670.
- [36] a) W. Y. Li, Q. F. Zhang, G. Y. Zheng, Z. W. Seh, H. B. Yao, Y. Cui, *Nano Lett.* **2013**, *13*, 5534; b) Y. Yang, G. H. Yu, J. J. Cha, H. Wu, M. Vosgueritchian, Y. Yao, Z. A. Bao, Y. Cui, *ACS Nano* **2011**, *5*, 9187; c) J. L. Wang, Y. S. He, J. Yang, *Adv. Mater.* **2015**, *27*, 569.
- [37] H.-J. Peng, G. Zhang, X. Chen, Z.-W. Zhang, W.-T. Xu, J.-Q. Huang, Q. Zhang, *Angew. Chem., Int. Ed.* **2016**, *55*, 12990.
- [38] Q. Pang, D. Kundu, M. Cuisinier, L. F. Nazar, *Nat. Commun.* **2014**, *5*, 4759.
- [39] X. Y. Tao, J. G. Wang, Z. G. Ying, Q. X. Cai, G. Y. Zheng, Y. P. Gan, H. Huang, Y. Xia, C. Liang, W. K. Zhang, Y. Cui, *Nano Lett.* **2014**, *14*, 5288.
- [40] Z. Yuan, H.-J. Peng, T.-Z. Hou, J.-Q. Huang, C.-M. Chen, D.-W. Wang, X.-B. Cheng, F. Wei, Q. Zhang, *Nano Lett.* **2016**, *16*, 519.
- [41] M.-S. Song, S.-C. Han, H.-S. Kim, J.-H. Kim, K.-T. Kim, Y.-M. Kang, H.-J. Ahn, S. Dou, J.-Y. Lee, *J. Electrochem. Soc.* **2004**, *151*, A791.
- [42] X. L. Ji, S. Evers, R. Black, L. F. Nazar, *Nat. Commun.* **2011**, *2*, 325.
- [43] Z. Yang, D. Choi, S. Kerisit, K. M. Rosso, D. Wang, J. Zhang, G. Graff, J. Liu, *J. Power Sources* **2009**, *192*, 588.
- [44] M. Yu, J. Ma, H. Song, A. Wang, F. Tian, Y. Wang, H. Qiu, R. Wang, *Energy Environ. Sci.* **2016**, *9*, 1495.
- [45] S. Evers, T. Yim, L. F. Nazar, *J. Phys. Chem. C* **2012**, *116*, 19653.
- [46] C. Z. Yuan, S. Q. Zhu, H. Cao, L. R. Hou, J. D. Lin, *Nanotechnology* **2016**, *27*, 045403.
- [47] Z. W. Seh, W. Y. Li, J. J. Cha, G. Y. Zheng, Y. Yang, M. T. McDowell, P. C. Hsu, Y. Cui, *Nat. Commun.* **2013**, *4*, 1331.

- [48] J. Y. Li, B. Ding, G. Y. Xu, L. R. Hou, X. G. Zhang, C. Z. Yuan, *Nanoscale* **2013**, 5, 5743.
- [49] X. Z. Ma, B. Jin, H. Y. Wang, J. Z. Hou, X. Bin Zhong, H. H. Wang, P. M. Xin, *J. Electroanal. Chem.* **2015**, 736, 127.
- [50] Q. Li, Z. Zhang, K. Zhang, L. Xu, J. Fang, Y. Q. Lai, J. Li, *J. Solid State Electron.* **2013**, 17, 2959.
- [51] K. Y. Xie, Y. Z. Han, W. F. Wei, H. R. Yu, C. B. Zhang, J. G. Wang, W. Lu, B. Q. Wei, *RSC Adv.* **2015**, 5, 77348.
- [52] Z. Liang, G. Y. Zheng, W. Y. Li, Z. W. Seh, H. B. Yao, K. Yan, D. S. Kong, Y. Cui, *ACS Nano* **2014**, 8, 5249.
- [53] Z.-Z. Yang, H.-Y. Wang, L. Lu, C. Wang, X.-B. Zhong, J.-G. Wang, Q.-C. Jiang, *Sci. Rep.* **2016**, 6, 22990.
- [54] J. Y. Hwang, H. M. Kim, S. K. Lee, J. H. Lee, A. Abouimrane, M. A. Khaleel, I. Belharouak, A. Manthiram, Y. K. Sun, *Adv. Energy Mater.* **2016**, 6, 1501480.
- [55] F. Wu, J. Li, Y. F. Tian, Y. F. Su, J. Wang, W. Yang, N. Li, S. Chen, L. Y. Bao, *Sci. Rep.* **2015**, 5, 13340.
- [56] X. H. Liang, C. C. Ye, L. Shi, Q. Q. Song, *Int. J. Electrochem. Sci.* **2014**, 9, 6677.
- [57] H. Q. Wang, S. Li, D. Li, Z. X. Chen, H. K. Liu, Z. P. Guo, *Energy* **2014**, 75, 597.
- [58] Z. Zhang, Q. Li, K. Zhang, W. Chen, Y. Q. Lai, J. Li, *J. Power Sources* **2015**, 290, 159.
- [59] a) M. Setvin, U. Aschauer, P. Scheiber, Y.-F. Li, W. Hou, M. Schmid, A. Selloni, U. Diebold, *Science* **2013**, 341, 988; b) U. Diebold, *Surf. Sci. Rep.* **2003**, 48, 53.
- [60] X. Liang, C. Hart, Q. Pang, A. Garsuch, T. Weiss, L. F. Nazar, *Nat. Commun.* **2015**, 6, 5682.
- [61] Y. Liu, J. Wei, Y. Tian, S. Yan, *J. Mater. Chem. A* **2015**, 3, 19000.
- [62] Z. Li, J. T. Zhang, X. W. Lou, *Angew. Chem., Int. Ed.* **2015**, 53, 12886.
- [63] X. Liang, C. Y. Kwok, F. Lodi-Marzano, Q. Pang, M. Cuisinier, H. Huang, C. J. Hart, D. Houtarde, K. Kaup, H. Sommer, T. Brezesinski, J. Janek, L. Nazar, *Adv. Energy Mater.* **2016**, 6, 1501636.
- [64] X. Liang, L. F. Nazar, *ACS Nano* **2016**, 10, 4192.
- [65] J. Lee, T. Hwang, Y. Lee, J. K. Lee, W. Choi, *Mater. Lett.* **2015**, 158, 132.
- [66] S. P. Wang, Z. G. Yang, H. Y. Zhang, H. B. Tan, J. X. Yu, J. P. Wu, *Electrochim. Acta* **2013**, 106, 307.
- [67] Y. Fu, Y. Wan, H. Xia, X. Wang, *J. Power Sources* **2012**, 213, 338.
- [68] Q. Fan, W. Liu, Z. Weng, Y. M. Sun, H. L. Wang, *J. Am. Chem. Soc.* **2015**, 137, 12946.
- [69] H. Tang, S. S. Yao, M. X. Jing, X. Wu, J. L. Hou, X. Y. Qian, D. W. Rao, X. Q. Shen, X. M. Xi, K. S. Xiao, *J. Alloys Compd.* **2015**, 650, 351.
- [70] Y. Zhang, Y. Zhao, A. Yermukhambetova, Z. Bakenov, P. Chen, *J. Mater. Chem. A* **2013**, 1, 295.
- [71] Y. Zhang, X. Wu, H. Feng, L. Wang, A. Zhang, T. Xia, H. Dong, *Int. J. Hydrogen Energy* **2009**, 34, 1556.
- [72] B. Campbell, J. Bell, H. H. Bay, Z. Favors, R. Ionescu, C. S. Ozkan, M. Ozkan, *Nanoscale* **2015**, 7, 7051.
- [73] K. T. Lee, R. Black, T. Yim, X. L. Ji, L. F. Nazar, *Adv. Energy Mater.* **2012**, 2, 1490.
- [74] Y. H. Qu, Z. A. Zhang, Y. Q. Lai, Y. X. Liu, J. Li, *Solid State Ionics* **2015**, 274, 71.
- [75] M. P. Yu, W. J. Yuan, C. Li, J. D. Hong, G. Q. Shi, *J. Mater. Chem. A* **2014**, 2, 7360.
- [76] X. H. Liang, C. C. Ye, Y. S. Liu, T. J. Liu, L. Shi, in *Energy Development, Pts 1–4*, Vol. 860–863, (Eds: Q. Xu, Y. Li, X. Yang), Trans Tech Publications Ltd, Stafa-Zurich, Switzerland **2014**, p. 952.
- [77] X. Li, J. Liu, B. Q. Wang, M. N. Banis, B. W. Xiao, R. Y. Li, T. K. Sham, X. L. Sun, *RSC Adv.* **2014**, 4, 27126.
- [78] F. G. Sun, J. T. Wang, D. H. Long, W. M. Qiao, L. C. Ling, C. X. Lv, R. Cai, *J. Mater. Chem. A* **2013**, 1, 13283.
- [79] Q. T. Qu, T. Gao, H. Y. Zheng, Y. Wang, X. Y. Li, X. X. Li, J. M. Chen, Y. Y. Han, J. Shao, H. H. Zheng, *Adv. Mater. Interfaces* **2015**, 2, 1500048.
- [80] a) M.-S. Kim, E. S. Shin, J.-S. Kim, W. I. Cho, S. H. Oh, *J. Electroceram.* **2014**, 33, 142; b) L. Kong, Y. Handa, I. Taniguchi, *Mater. Res. Bull.* **2016**, 73, 164.
- [81] L. P. Zhang, Y. F. Wang, S. Q. Gou, J. H. Zeng, *J. Phys. Chem. C* **2015**, 119, 28721.
- [82] G. Q. Ma, Z. Y. Wen, Q. S. Wang, J. Jin, X. W. Wu, J. C. Zhang, *J. Inorg. Mater.* **2015**, 30, 913.
- [83] a) N. Azimi, Z. Xue, I. Bloom, M. L. Gordin, D. H. Wang, T. Daniel, C. Takoudis, Z. C. Zhang, *ACS Appl. Mater. Interfaces* **2015**, 7, 9169; b) Y. Zhou, C. G. Zhou, Q. Y. Li, C. J. Yan, B. Han, K. S. Xia, Q. Gao, J. P. Wu, *Adv. Mater.* **2015**, 27, 3774.
- [84] S. Rehman, S. Guo, Y. Hou, *Adv. Mater.* **2016**, 28, 3167.
- [85] C. C. Zhao, C. Shen, F. X. Xin, Z. X. Sun, W. Q. Han, *Mater. Lett.* **2014**, 137, 52.
- [86] M. P. Yu, A. J. Wang, F. Y. Tian, H. Q. Song, Y. S. Wang, C. Li, J. D. Hong, G. Q. Shi, *Nanoscale* **2015**, 7, 5292.
- [87] X. H. Liang, Q. Q. Song, Y. S. Liu, H. Liu, *Int. J. Electrochem. Sci.* **2015**, 10, 9333.
- [88] H. Cheng, S. P. Wang, D. Tao, M. Wang, *Funct. Mater. Lett.* **2014**, 7, 1450020.
- [89] L. F. Xiao, Y. L. Cao, J. Xiao, B. Schwenzer, M. H. Engelhard, L. V. Saraf, Z. M. Nie, G. J. Exarhos, J. Liu, *Adv. Mater.* **2012**, 24, 1176.
- [90] M. Hagen, D. Hanselmann, K. Ahlbrecht, R. Maca, D. Gerber, J. Tubke, *Adv. Energy Mater.* **2015**, 5, 1401986.
- [91] a) J.-Q. Huang, Q. Zhang, F. Wei, *Energy Storage Mater.* **2015**, 1, 127; b) N. Deng, W. Kang, Y. Liu, J. Ju, D. Wu, L. Li, B. S. Hassan, B. Cheng, *J. Power Sources* **2016**, 331, 132.
- [92] a) Y. S. Su, A. Manthiram, *Nat. Commun.* **2012**, 3, 1166; b) S. H. Chung, A. Manthiram, *Adv. Mater.* **2014**, 26, 7352.
- [93] a) J. Q. Huang, Q. Zhang, H. J. Peng, X. Y. Liu, W. Z. Qian, F. Wei, *Energy Environ. Sci.* **2014**, 7, 347; b) X. W. Yu, J. Joseph, A. Manthiram, *J. Mater. Chem. A* **2015**, 3, 15683; c) I. Bauer, S. Thieme, J. Bruckner, H. Althues, S. Kaskel, *J. Power Sources* **2014**, 251, 417.
- [94] J. Q. Huang, T. Z. Zhuang, Q. Zhang, H. J. Peng, C. M. Chen, F. Wei, *ACS Nano* **2015**, 9, 3002.
- [95] a) G. M. Zhou, L. Li, D. W. Wang, X. Y. Shan, S. F. Pei, F. Li, H. M. Cheng, *Adv. Mater.* **2015**, 27, 641; b) G. M. Zhou, S. F. Pei, L. Li, D. W. Wang, S. G. Wang, K. Huang, L. C. Yin, F. Li, H. M. Cheng, *Adv. Mater.* **2014**, 26, 625.
- [96] a) Y. B. Zhang, L. X. Miao, J. Ning, Z. C. Xiao, L. Hao, B. Wang, L. J. Zhi, *2D Mater.* **2015**, 2, 024013; b) H.-J. Peng, Z.-W. Zhang, J.-Q. Huang, G. Zhang, J. Xie, W.-T. Xu, J.-L. Shi, X. Chen, X.-B. Cheng, Q. Zhang, *Adv. Mater.* **2016**, 28, 9551.
- [97] T. Z. Zhuang, J. Q. Huang, H. J. Peng, L. Y. He, X. B. Cheng, C. M. Chen, Q. Zhang, *Small* **2016**, 12, 381.
- [98] W. Li, J. Hicks-Garner, J. Wang, J. Liu, A. F. Gross, E. Sherman, J. Graetz, J. J. Vajo, P. Liu, *Chem. Mater.* **2014**, 26, 3403.
- [99] Z. B. Xiao, Z. Yang, L. Wang, H. G. Nie, M. E. Zhong, Q. Q. Lai, X. J. Xu, L. J. Zhang, S. M. Huang, *Adv. Mater.* **2015**, 27, 2891.
- [100] Q. Xu, G. C. Hu, H. L. Bi, H. F. Xiang, *Ionics* **2015**, 21, 981.
- [101] G. M. Zhou, Y. B. Zhao, C. X. Zu, A. Manthiram, *Nano Energy* **2015**, 12, 240.
- [102] G. Y. Xu, J. R. Yuan, X. Y. Tao, B. Ding, H. Dou, X. H. Yan, Y. Xiao, X. G. Zhang, *Nano Res.* **2015**, 8, 3066.
- [103] Z. Y. Zhang, Y. Q. Lai, Z. A. Zhang, K. Zhang, J. E. Li, *Electrochim. Acta* **2014**, 129, 55.
- [104] H. B. Yao, K. Yan, W. Y. Li, G. Y. Zheng, D. S. Kong, Z. W. Seh, V. K. Narasimhan, Z. Liang, Y. Cui, *Energy Environ. Sci.* **2014**, 7, 3381.

- [105] X. G. Han, Y. H. Xu, X. Y. Chen, Y. C. Chen, N. Weadock, J. Y. Wan, H. L. Zhu, Y. L. Liu, H. Q. Li, G. Rubloff, C. S. Wang, L. B. Hu, *Nano Energy* **2013**, *2*, 1197.
- [106] H. K. Jing, L. L. Kong, S. Liu, G. R. Li, X. P. Gao, *J. Mater. Chem. A* **2015**, *3*, 12213.
- [107] Q. S. Wang, Z. Y. Wen, J. H. Yang, J. Jin, X. Huang, X. W. Wu, J. D. Han, *J. Power Sources* **2016**, *306*, 347.
- [108] W. Ahn, S. N. Lim, D. U. Lee, K. B. Kim, Z. W. Chen, S. H. Yeon, *J. Mater. Chem. A* **2015**, *3*, 9461.
- [109] L. Wang, J. Y. Liu, S. Haller, Y. G. Wang, Y. Y. Xia, *Chem. Commun.* **2015**, *51*, 6996.
- [110] W. K. Zhang, C. Lin, S. Cong, J. Y. Hou, B. Liu, F. X. Geng, J. Jin, M. H. Wu, Z. G. Zhao, *RSC Adv* **2016**, *6*, 15234.
- [111] a) R. G. Cao, W. Xu, D. P. Lv, J. Xiao, J. G. Zhang, *Adv. Energy Mater.* **2015**, *5*, 1402273; b) C. Yan, X.-B. Cheng, C.-Z. Zhao, J.-Q. Huang, S.-T. Yang, Q. Zhang, *J. Power Sources* **2016**, *327*, 212.
- [112] D. Aurbach, E. Pollak, R. Elazari, G. Salitra, C. S. Kelley, J. Affinito, *J. Electrochem. Soc.* **2009**, *156*, A694.
- [113] a) C.-Z. Zhao, X.-B. Cheng, R. Zhang, H.-J. Peng, J.-Q. Huang, R. Ran, Z.-H. Huang, F. Wei, Q. Zhang, *Energy Storage Mater.* **2016**, *3*, 77; b) W. Y. Li, H. B. Yao, K. Yan, G. Y. Zheng, Z. Liang, Y. M. Chiang, Y. Cui, *Nat. Commun.* **2015**, *6*, 7436.
- [114] F. Ding, W. Xu, G. L. Graff, J. Zhang, M. L. Sushko, X. L. Chen, Y. Y. Shao, M. H. Engelhard, Z. M. Nie, J. Xiao, X. J. Liu, P. V. Sushko, J. Liu, J. G. Zhang, *J. Am. Chem. Soc.* **2013**, *135*, 4450.
- [115] Y. Lu, Z. Tu, L. A. Archer, *Nat. Mater.* **2014**, *13*, 961.
- [116] a) F. Wu, J. Qian, R. J. Chen, J. Lu, L. Li, H. M. Wu, J. Z. Chen, T. Zhao, Y. S. Ye, K. Amine, *ACS Appl. Mater. Interfaces* **2014**, *6*, 15542; b) C. X. Zu, N. Azimi, Z. C. Zhang, A. Manthiram, *J. Mater. Chem. A* **2015**, *3*, 14864.
- [117] L. M. Suo, Y. S. Hu, H. Li, M. Armand, L. Q. Chen, *Nat. Commun.* **2013**, *4*, 1481.
- [118] M. Wu, Z. Wen, J. Jin, B. V. R. Chowdari, *ACS Appl. Mater. Interfaces* **2016**, *8*, 16386.
- [119] K. Yan, H. W. Lee, T. Gao, G. Y. Zheng, H. B. Yao, H. T. Wang, Z. D. Lu, Y. Zhou, Z. Liang, Z. F. Liu, S. Chu, Y. Cui, *Nano Lett.* **2014**, *14*, 6016.
- [120] G. Y. Zheng, S. W. Lee, Z. Liang, H. W. Lee, K. Yan, H. B. Yao, H. T. Wang, W. Y. Li, S. Chu, Y. Cui, *Nat. Nanotechnol.* **2014**, *9*, 618.
- [121] a) C.-P. Yang, Y.-X. Yin, S.-F. Zhang, N.-W. Li, Y.-G. Guo, *Nat. Commun.* **2015**, *6*, 8058; b) L.-L. Lu, J. Ge, J.-N. Yang, S.-M. Chen, H.-B. Yao, F. Zhou, S.-H. Yu, *Nano Lett.* **2016**, *16*, 4431.
- [122] Q. Yun, Y.-B. He, W. Lv, Y. Zhao, B. Li, F. Kang, Q.-H. Yang, *Adv. Mater.* **2016**, *28*, 6932.
- [123] X.-B. Cheng, H.-J. Peng, J.-Q. Huang, R. Zhang, C.-Z. Zhao, Q. Zhang, *ACS Nano* **2015**, *9*, 6373.
- [124] D. C. Lin, Y. Y. Liu, Z. Liang, H. W. Lee, J. Sun, H. T. Wang, K. Yan, J. Xie, Y. Cui, *Nat. Nanotechnol.* **2016**, *11*, 626.
- [125] Z. Liang, D. C. Lin, J. Zhao, Z. D. Lu, Y. Y. Liu, C. Liu, Y. Y. Lu, H. T. Wang, K. Yan, X. Y. Tao, Y. Cui, *Proc. Natl. Acad. Sci. USA* **2016**, *113*, 2862.
- [126] X. B. Cheng, H. J. Peng, J. Q. Huang, F. Wei, Q. Zhang, *Small* **2014**, *10*, 4257.
- [127] Z. Y. Tu, P. Nath, Y. Y. Lu, M. D. Tikekar, L. A. Archer, *Acc. Chem. Res.* **2015**, *48*, 2947.
- [128] X. B. Cheng, T. Z. Hou, R. Zhang, H. J. Peng, C. Z. Zhao, J. Q. Huang, Q. Zhang, *Adv. Mater.* **2016**, *28*, 2888.
- [129] R. Song, R. Fang, L. Wen, Y. Shi, S. Wang, F. Li, *J. Power Sources* **2016**, *307*, 179.
- [130] A. C. Kozen, C.-F. Lin, A. J. Pearse, M. A. Schroeder, X. Han, L. Hu, S.-B. Lee, G. W. Rubloff, M. Noked, *ACS Nano* **2015**, *9*, 5884.
- [131] K. Fu, Y. Gong, J. Dai, A. Gong, X. Han, Y. Yao, C. Wang, Y. Wang, Y. Chen, C. Yan, Y. Li, E. D. Wachsman, L. Hu, *Proc. Natl. Acad. Sci. USA* **2016**, *113*, 7094.
- [132] X. Liang, A. Garsuch, L. F. Nazar, *Angew. Chem., Int. Ed.* **2015**, *54*, 3907.
- [133] Q. Pang, D. Kundu, L. F. Nazar, *Mater. Horiz.* **2016**, *3*, 130.
- [134] S. S. Zhang, D. T. Tran, *J. Mater. Chem. A* **2016**, *4*, 4371.
- [135] X. Li, L. Chu, Y. Wang, L. Pan, *Mater. Sci. Eng. B* **2016**, *205*, 46.
- [136] N. N. Greenwood, A. Earnshaw, *Chemistry of the Elements*, Elsevier, UK **2012**.
- [137] Z. W. Seh, J. H. Yu, W. Y. Li, P. C. Hsu, H. T. Wang, Y. M. Sun, H. B. Yao, Q. F. Zhang, Y. Cui, *Nat. Commun.* **2014**, *5*, 5017.
- [138] Q. F. Zhang, Y. P. Wang, Z. W. Seh, Z. H. Fu, R. F. Zhang, Y. Cui, *Nano Lett.* **2015**, *15*, 3780.
- [139] a) M. S. Faber, M. A. Lukowski, Q. Ding, N. S. Kaiser, S. Jin, *J. Phys. Chem. C* **2014**, *118*, 21347; b) M. S. Faber, R. Dzedzic, M. A. Lukowski, N. S. Kaiser, Q. Ding, S. Jin, *J. Am. Chem. Soc.* **2014**, *136*, 10053.
- [140] Z. Ma, Z. Li, K. Hu, D. Liu, J. Huo, S. Wang, *J. Power Sources* **2016**, *325*, 71.
- [141] L. Ma, S. Y. Wei, H. L. L. Zhuang, K. E. Hendrickson, R. G. Hennig, L. A. Archer, *J. Mater. Chem. A* **2015**, *3*, 19857.
- [142] Y. S. Su, A. Manthiram, *J. Power Sources* **2014**, *270*, 101.
- [143] J. D. Liu, X. S. Zheng, Z. F. Shi, S. Q. Zhang, *Ionics* **2014**, *20*, 659.
- [144] K. Sun, D. Su, Q. Zhang, D. C. Bock, A. C. Marschilok, K. J. Takeuchi, E. S. Takeuchi, H. Gan, *J. Electrochem. Soc.* **2015**, *162*, A2834.
- [145] L. Chen, J. D. Liu, S. Q. Zhang, *J. Inorg. Mater.* **2013**, *28*, 1127.
- [146] X. Li, Y. Lu, Z. Hou, W. Zhang, Y. Zhu, Y. Qian, J. Liang, Y. Qian, *ACS Appl. Mater. Interfaces* **2016**, *8*, 19550.
- [147] Y. Lu, X. Li, J. Liang, L. Hu, Y. Zhu, Y. Qian, *Nanoscale* **2016**, *8*, 17616.
- [148] D. P. Lv, J. M. Zheng, Q. Y. Li, X. Xie, S. Ferrara, Z. M. Nie, L. B. Mehdii, N. D. Browning, J. G. Zhang, G. L. Graff, J. Liu, Y. Xiao, *Adv. Energy Mater.* **2015**, *5*, 1402290.
- [149] a) Z. Yuan, H. J. Peng, J. Q. Huang, X. Y. Liu, D. W. Wang, X. B. Cheng, Q. Zhang, *Adv. Funct. Mater.* **2014**, *24*, 6105; b) G. J. Hu, C. Xu, Z. H. Sun, S. G. Wang, H. M. Cheng, F. Li, W. C. Ren, *Adv. Mater.* **2016**, *28*, 1603; c) W. C. Du, Y. X. Yin, X. X. Zeng, J. L. Shi, S. F. Zhang, L. J. Wan, Y. G. Guo, *ACS Appl. Mater. Interfaces* **2016**, *8*, 3584.
- [150] a) J. Q. Huang, B. A. Zhang, Z. L. Xu, S. Abouali, M. A. Garakani, J. Q. Huang, J. K. Kim, *J. Power Sources* **2015**, *285*, 43; b) X. Q. Zhao, M. Liu, Y. Chen, B. Hou, N. Zhang, B. B. Chen, N. Yang, K. Chen, J. L. Li, L. A. An, *J. Mater. Chem. A* **2015**, *3*, 7870.
- [151] J. Jiang, J. H. Zhu, W. Ai, X. L. Wang, Y. L. Wang, C. J. Zou, W. Huang, T. Yu, *Nat. Commun.* **2015**, *6*, 8622.
- [152] a) J. M. Zheng, J. Tian, D. X. Wu, M. Gu, W. Xu, C. M. Wang, F. Gao, M. H. Engelhard, J. G. Zhang, J. Liu, J. Xiao, *Nano Lett.* **2014**, *14*, 2345; b) J. W. Zhou, R. Li, X. X. Fan, Y. F. Chen, R. D. Han, W. Li, J. Zheng, B. Wang, X. G. Li, *Energy Environ. Sci.* **2014**, *7*, 2715.
- [153] H. B. Yao, G. Y. Zheng, P. C. Hsu, D. S. Kong, J. J. Cha, W. Y. Li, Z. W. Seh, M. T. McDowell, K. Yan, Z. Liang, V. K. Narasimhan, Y. Cui, *Nat. Commun.* **2014**, *5*, 3943.
- [154] H. N. Chen, Q. L. Zou, Z. J. Liang, H. Liu, Q. Li, Y. C. Lu, *Nat. Commun.* **2015**, *6*, 5877.
- [155] Y. Yang, G. Y. Zheng, Y. Cui, *Energy Environ. Sci.* **2013**, *6*, 1552.
- [156] a) Y. Yang, M. T. McDowell, A. Jackson, J. J. Cha, S. S. Hong, Y. Cui, *Nano Lett.* **2010**, *10*, 1486; b) Z. W. Seh, H. T. Wang, P. C. Hsu, Q. F. Zhang, W. Y. Li, G. Y. Zheng, H. B. Yao, Y. Cui, *Energy Environ. Sci.* **2014**, *7*, 672; c) Z. W. Seh, H. T. Wang, N. Liu, G. Y. Zheng,

- W. Y. Li, H. B. Yao, Y. Cui, *Chem Sci* **2014**, *5*, 1396; d) Y. Z. Fu, Y. S. Su, A. Manthiram, *Adv. Energy Mater.* **2014**, *4*, 1300655.
- [157] a) S. H. Chung, A. Manthiram, *Adv. Funct. Mater.* **2014**, *24*, 5299; b) H. J. Peng, D. W. Wang, J. Q. Huang, X. B. Cheng, Z. Yuan, F. Wei, Q. Zhang, *Adv. Sci.* **2016**, *3*, 1500268.
- [158] H. B. Yao, G. Y. Zheng, P. C. Hsu, D. S. Kong, J. J. Cha, W. Y. Li, Z. W. Seh, M. T. McDowell, K. Yan, Z. Liang, V. K. Narasimhan, Y. Cui, *Nat. Commun.* **2014**, *5*, 9.
- [159] W. Y. Li, Z. Liang, Z. D. Lu, X. Y. Tao, K. Liu, H. B. Yao, Y. Cui, *Nano Lett.* **2015**, *15*, 7394.
- [160] C. J. Hart, M. Cuisinier, X. Liang, D. Kundu, A. Garsuch, L. F. Nazar, *Chem. Commun.* **2015**, *51*, 2308.
- [161] a) T. Z. Hou, H. J. Peng, J. Q. Huang, Q. Zhang, B. Li, *2D Mater.* **2015**, *2*, 014011; b) L. C. Yin, J. Liang, G. M. Zhou, F. Li, R. Saito, H. M. Cheng, *Nano Energy* **2016**, *25*, 203; c) T. Z. Hou, X. Chen, H. J. Peng, J. Q. Huang, B. Q. Li, Q. Zhang, B. Li, *Small* **2016**, *12*, 3283.
- [162] X. Y. Tao, J. G. Wang, C. Liu, H. T. Wang, H. B. Yao, G. Y. Zheng, Z. W. Seh, Q. X. Cai, W. Y. Li, G. M. Zhou, C. X. Zu, Y. Cui, *Nat. Commun.* **2016**, *7*, 11203.
- [163] H. T. Wang, Q. F. Zhang, H. B. Yao, Z. Liang, H. W. Lee, P. C. Hsu, G. Y. Zheng, Y. Cui, *Nano Lett.* **2014**, *14*, 7138.
- [164] A. Grimaud, W. Hong, Y. Shao-Horn, J.-M. Tarascon, *Nat. Mater.* **2016**, *15*, 121.
- [165] A. White, *MRS Bull.* **2012**, *37*, 715.